Author's personal copy

Available online at www.sciencedirect.com
ScienceDirect
Geochimica et Cosmochimica Acta 72 (2008) 2217–2235
Geochimica et Cosmochimica Acta
www.elsevier.com/locate/gca

# A depleted, not ideally chondritic bulk Earth: The explosive-volcanic basalt loss hypothesis

Paul H. Warren

*Institute of Geophysics, UCLA, Los Angeles, CA 90095-1567, USA*

Received 30 July 2007; accepted in revised form 19 November 2007; available online 26 February 2008

**Abstract**

It has long been customary to assume that in the bulk composition of the Earth, all refractory-lithophile elements (including major oxides $Al_2O_3$ and CaO, all of the REE, and the heat-producing elements Th and U) occur in chondritic, bulk solar system, proportion to one another. Recently, however, Nd-isotopic studies (most notably Boyet M. and Carlson R. W. (2006) A new geochemical model for the Earth's mantle inferred from $^{146}Sm$–$^{142}Nd$ systematics. *Earth Planet. Sci. Lett.* **250**, 254–268) have suggested that at least the outer portion of the planet features a Nd/Sm ratio depleted to ~0.93 times the chondritic ratio. The primary reaction to this type of evidence has been to invoke a "hidden" reservoir of enriched matter, sequestered into the deepest mantle as a consequence of primordial differentiation. I propose a hypothesis that potentially explains the evidence for Nd/Sm depletion in a very different way. Among the handful of major types of differentiated asteroidal meteorites, two (ureilites and aubrites) are ultramafic restites so consistently devoid of plagioclase that meteoriticists were once mystified as to how all the complementary plagioclase-rich matter (basalt) was lost. The explanation appears to be basalt loss by graphite-fueled explosive volcanism on roughly 100-km sized planetesimals; with the dispersiveness of the process dramatically enhanced, relative to terrestrial experience, because the pyroclastic gases expand into vacuous space (Wilson L. and Keil K. (1991) Consequences of explosive eruptions on small Solar System bodies: the case of the missing basalts on the aubrite parent body. *Earth Planet. Sci. Lett.* **104**, 505–512). By analogy with lunar pyroclastic products, the typical size of pyroclastic melt/glass droplets under these circumstances will be roughly 0.1 mm. Once separated from an asteroidal or planetesimal gravitational field, droplets of this size will generally spiral toward the Sun, rather than reaccrete, because drag forces such the Poynting–Robertson effect quickly modify their orbits (the semimajor axis, in a typical scenario, is reduced by several hundred km during the first trip around the Sun). Assuming a similar process occurred on many of the Earth's precursor planetesimals while they were still roughly 100 km in diameter, the net effect would be a depleted composition for the final Earth. I have modeled the process of trace-element depletion in the planetesimal mantles, assuming the partial melting was nonmodal and either batch or dynamic in terms of the melt-removal style. Assuming the process is moderately efficient, typical final-Earth Nd/Sm ratios are 0.93–0.96 times chondritic. Depletion is enhanced by a relatively low assumed residual porosity in batch-melting scenarios, but dampened by a relatively high value for "continuous" residue porosity in dynamic melting scenarios. Pigeonite in the source matter has a dampening effect on depletion. There are important side effects to the Nd/Sm depletion. The heat-producing elements, Th, U and K, might be severely depleted. The $Eu/Eu^*$ ratio of the planet is unlikely to remain precisely chondritic. One of the most inevitable side effects, depletion of the Al/Ca ratio, is consistent with an otherwise puzzling aspect of the composition of the upper mantle. A perfectly undepleted composition for the bulk Earth is dubious.
© 2008 Elsevier Ltd. All rights reserved.

## 1. INTRODUCTION

Planetary scientists generally assume that except for volatile elements, the bulk composition of a planet, until proven otherwise, is "chondritic," meaning similar to the bulk

*E-mail address:* pwarren@ucla.edu

0016-7037/$ - see front matter © 2008 Elsevier Ltd. All rights reserved.
doi:10.1016/j.gca.2007.11.038

Author's personal copy



solar system (the Sun) as represented by primitive meteorites. In detail, as has long been known (Urey, 1952), planetary bulk compositions are not chondritic. Volatility-related depletions are evident even among chondrites (Wasson and Kallemeyn, 1988), and highly volatile elements presumably undergo further depletion during the igneous processing of planetesimals (Mittlefehldt et al., 1998). Correlated incompatible elements such as K and U manifest obvious bulk-planetary differences between, for example, volatile-rich (high-K/U) Mars and the volatile-poor (low-K/U) Moon; and metal/silicate fractionation left the Moon and Mercury with far from chondritic Fe/Si ratios (and presumably nonchondritic siderophile/lithophile element ratios) (Taylor, 2001). Major collisional processes hold obvious potential for inducing metal-silicate fractionation, and recent work by Asphaug et al. (2006) indicates that differentiation by disruptive collision may be more complex, and diverse in its consequences, than previously suspected. For the many nonvolatile-lithophile elements, however, the usual presumption is that in bulk planets each of these elements occurs in precise chondritic proportion to all other such elements.

Among this category of nonvolatile-lithophile elements, the 15 geochemically coherent rare-earth elements (REE), including samarium and neodymium, are exemplary, being both highly refractory (in gas-involved reactions) and highly lithophile. However, recent high-precision measurements of $^{142}$Nd (formed by decay of short-lived $^{146}$Sm) indicate that for much, if not all, of Earth's mantle, the Nd/Sm ratio is decidedly depleted versus the narrow range defined by all known chondrites (Boyet and Carlson, 2005, 2006). The upper-mantle source regions of mid-ocean ridge basalts (MORB), komatiites, and a variety of other igneous rocks, consistently have $^{142}$Nd/$^{144}$Nd about 20 μ (ppm) higher than the well-defined mean $^{142}$Nd/$^{144}$Nd of a variety of chondrites; and in order to evolve a 20 μ $^{142}$Nd/$^{144}$Nd excess, even assuming the maximum conceivable age (4.566 Ga) for Sm–Nd fractionation, a reservoir must have Sm/Nd 1.073 times the mean chondritic value; i.e., Nd/Sm (wt ratio) depleted to 0.932 times the mean chondritic value (Boyet and Carlson, 2005, 2006).

One model to account for evidence of upper-mantle Nd/Sm depletion is to assume the existence of a deep mantle reservoir with enriched Nd/Sm (Chase and Patchett, 1988; Boyet et al., 2003; Caro et al., 2003; Boyet and Carlson, 2005, 2006). Albarède (2006) has opined that this inference (i.e., that such a lower-mantle reservoir exists, in a state of effective, long-term, stable isolation from the upper mantle) appears "inescapable." A lower-mantle enriched reservoir conceivably formed by some highly unusual subduction process in the aftermath of primordial differentiation (e.g., Boyet et al., 2003; Samuel and Farnetani, 2003; Tolstikhin et al., 2006). Still, it hardly seems inevitable that Earth's early differentiation led to a permanent, isolating burial of the late-stage enriched matter that presumably originally formed near the surface.

I shall argue that the chondritic bulk-Earth paradigm does not necessarily hold for ratios such as Nd/Sm, because igneously differentiated carbon-rich asteroid-sized protoplanets (which plausibly comprised a major fraction of the eventual Earth-forming matter) are prone to engender depletion of light REE relative to heavy REE, along with a general of depletion of incompatible elements. This proposal challenges a long-canonical view, the presumption that the bulk-Earth complement of refractory-lithophile elements (including the REE) is chondritic. Yet it is hardly a novel proposal from the meteoritical perspective. Rather, it is a logical corollary from models that have been expounded, and little-challenged, for some 15 or 16 years, in relation to the differentiated asteroids that supplied two important classes of igneous meteorites, the ureilites and the aubrites (Wilson and Keil, 1991; Warren and Kallemeyn, 1992; Scott et al., 1993).

This new model assumes that Earth formed in large part from materials that were analogous to those differentiated meteorites, in that they passed through a stage in which as partially melted asteroid-sized bodies (e.g., Taylor et al., 1993; Hevey and Sanders, 2006; McCoy et al., 2006) they underwent carbon-fueled, basalt-depletive pyroclastic eruptions. The model also assumes that the Poynting–Robertson effect determined the ultimate fate of basaltic pyroclasts launched off the putative asteroid-sized protoplanets. The scenario of an important degree of basalt loss during planetesimal volcanism is admittedly far from certain, but I shall argue that it is plausible, even apart from the need to account for otherwise puzzling Nd isotopic results.

## 2. PREVIOUS METEORITE-BASED MODELS

Among the largest groups of nonmetallic igneous meteorites, the second and third most numerous groups (counting HEDs as a single group) are the ureilites, with well over 100 individual meteorites, and the aubrites, roughly 1/3 as numerous as the ureilites. Both ureilites and aubrites are generally modeled as ultramafic residues produced by partial melting (anatexis) of asteroidal mantles (Wilson and Keil, 1991; Warren and Kallemeyn, 1992; Scott et al., 1993). As collective samples of their parent asteroids, both ureilites and aubrites are impressively devoid of the basaltic matter that must have formed in association with these ultramafic residues. The lack of associated basalts began to appear significant as the numbers of meteorites burgeoned starting circa 1980 (when thousands of Antarctic and warm-desert finds began to be harvested and classified). At the same time, meteoriticists came to appreciate that important subsets of both groups are regolith breccias, as evidenced most definitively by solar-wind derived noble gases but also by diverse lithic clasts (for reviews on the geochemistry and petrology, see Keil, 1989 for aubrites; Kennedy et al., 1993, for ureilites). Regoliths, as shallow aggregates of randomly scattered debris from surface impacts, are expected to hold at least representative proportions of whatever basaltic crust existed during the cratering of the parent asteroid; so it is remarkable to find that even regolithic ureilites and aubrites are almost devoid of basaltic matter. Wilson and Keil (1991) proposed a specific and plausible model to account for the gross depletion of basalt from the aubrite parent asteroid. The same basic model was soon adapted for ureilites by Warren and Kallemeyn (1992) and Scott et al. (1993).

Author's personal copy



Wilson and Keil (1991) suggested that expansion of exsolving gas during eruptions of basaltic magmas into the vacuum around an asteroid may have entrained the eruptive basalt, in the form of small melt droplets, at such high velocity as to efficiently launch them beyond the gravitational Hill sphere of the asteroid. Assuming a fixed density $\rho$, an asteroid's escape velocity $v_{esc}$ is directly proportional to its radius $R$:

$$v_{esc} = [(8/3)\pi G\rho]^{0.5} R \quad (1)$$

where $G$ is the universal gravitation constant. Assuming $\rho = 3500\ \mathrm{kg\ m^{-3}}$, and taking the liberty of mixing length units, $v_{esc}$ in meters/second is conveniently equal to $1.40R$, for $R$ in the familiar units of kilometers.

The efficiency of this mechanism is sensitive to the sizes of the pyroclastic melt blobs (or droplets) that form as the explosion of the gas into the low-pressure environment above the asteroidal surface causes dispersal ("disruption" or "fragmentation") of the melt. Small melt blobs will be accelerated to (launched at) velocities very near the expansion velocity of the gas $u$, for which Wilson and Keil (1991) derived the expression,

$$u^2 = \frac{2nQT}{m}\frac{\gamma}{\gamma - 1}[1 - (P_a/P_d)^{(\gamma-1)/\gamma}] \quad (2)$$

where $n$ is the mass fraction of (exsolved) gas in the fragmentation-mixture, $Q$ is the universal gas constant, $T$ is the temperature, $m$ is the molecular weight of the gas phase, $\gamma$ is the ratio of specific heats of the gas ($\approx 4/3$), $P_a$ is the atmospheric pressure and $P_d$ is the pressure at which disruption occurs. For eruptions on atmosphereless bodies, the term in square brackets in (2) is virtually 1. The timescale for nebular gas clear-out is of order $10^6$–$10^7$ years (Cameron, 1995), comparable to the time-scale ($\sim$2–3 $\times$ $10^6$ years) for melting by decay of short-lived radionuclides (mainly $^{26}$Al), according to the models of Bizzarro et al. (2005) and Hevey and Sanders (2006). If nebular gas remained in the vicinity, $u$ would be reduced, but not by a large factor. For example, taking $P_a$ to be the estimated nebular midplane $P$ of $10^{-5}$ bar (see review by Wood, 2000) and assuming $P_d$ is of order 1 bar, the $u$ implied by (2) would be 0.97 times the atmosphere-free value. The overriding determinant of $u$ (for any given $m$, i.e., gas composition) is thus $n^{0.5}$. As discussed by Wilson and Keil (1991), (2) may underestimate $u$ by a factor of $\sim$2 if the expansion of the gas is isothermal rather than isentropic. Wilson and Keil (1991) assumed that the isentropic model (2) is more realistic, but Wilson and Keil (1997) argued that the isothermal model is probably more relevant for pyroclastic eruptions on an asteroid.

Wilson and Keil (1991) combined (1) and (2) to estimate, as a function of $R$, the "critical" volatile content $n_{crit}$ that suffices to accelerate (small) basaltic pyroclasts to a $u$ greater than $v_{esc}$. Their definition for $n_{crit}$ assumes conversion of $n$ into units of μg/g, along with gas properties of $\gamma = 4/3$ and $m = 30$. Diverse volatiles might have contributed significantly to the gas, but $CO_x$, with more CO than $CO_2$ and thus $m \approx 30$, as expected from burning of solid carbon (graphite), was probably preponderant. The relationship between $n_{crit}$ and asteroid radius derived by Wilson and Keil (1991, their Fig. 3) can be approximated as

$$n_{crit} = 0.5\ R^2 \quad (3)$$

for $R$ in km.

Other gases such as $SO_X$ or $N_2$ might have been significant. Although N is suitably abundant in the most volatile-rich types of chondrite (CI and CM contain $\sim$1500 μg/g), most chondrite types contain <100 μg/g (Wasson and Kallemeyn, 1988). Libourel et al. (2003) found that N solubility can be well over 1000 μg/g for basaltic melt at planetesimal pressures and extremely low, but plausibly relevant (near or below the CCO buffer), $fO_2$. Holzheid and Grove (2002) found that the solubility of S in silicate melts at the relevant $T$ ($\sim$1300 °C) is roughly 1500 μg/g. The effect of extremely low $fO_2$ on S solubility is unclear, and the effect of pressure is, for a planetesimal context, negligible. However, simple cooling of the magma as it vents would diminish the solubility and thus might, in time to be still relevant to the explosive dispersal of pyroclasts, release a significant proportion of $S_2$ (according to Zolotov and Fegley, 1999, at IW or below, the S gas species is preponderantly $S_2$; the proportion of $SO_2$ is negligible). Of course, $m \approx 64$ implies that for any given mass concentration, magmatic S has only about half the explosive-fuel potential as $CO_x$.

The reaction to form $CO_x$ is basically

$$C(\mathrm{graphite}) + x\mathrm{FeO}(\mathrm{melt}) = CO_x(\mathrm{gas}) + x\mathrm{Fe}(\mathrm{metal}) \quad (4)$$

where $x$ is between 1 and 2. Of course, a real-world process is slightly more complicated, with other multivalent cations (e.g., Cr) also involved in the redox reaction. At magmatic $T$ and close to the "buffer" equilibrium (4), $x$ is close to 1 (Warren and Kallemeyn, 1992). Since a gas phase exists

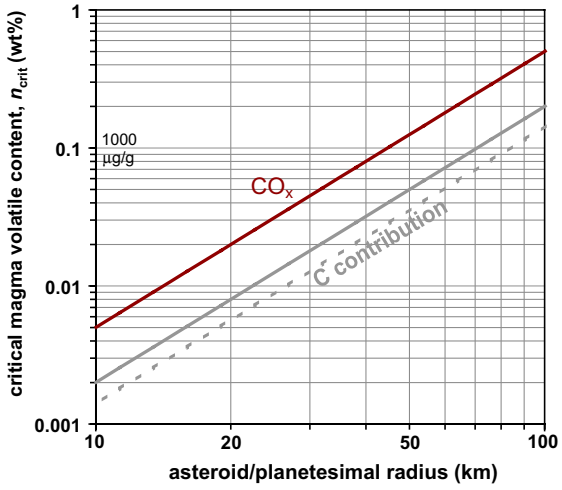


Fig. 1. The "critical" volatile content $n_{crit}$ that suffices to accelerate (small) basaltic pyroclasts to a velocity greater than $v_{esc}$, shown as a function of planetesimal or asteroid radius $R$. Grey curves show the equivalent contribution of elemental carbon, i.e., the proportion of graphite that must be entrained with the ascending melt and oxidized into $CO_x$ gas (assuming a $CO/CO_2$ molar ratio of 9), to yield $n_{crit}$, for both the isentropic (solid curve) and the isothermal (dashed curve) models.

Author's personal copy



only on the right side of (4), this process is extremely pressure-sensitive. The "buffer" $P$ is of order 10–100 bar, depending upon the *mg* ratio (=molar MgO/[MgO + FeO]) of the system (Warren and Kallemeyn, 1992).

The relationship between $n_{crit}$ and $R$ implied by (3) is illustrated in Fig. 1, where the contribution of elemental carbon needed to yield $n_{crit}$ (i.e., of graphite that must be entrained with the ascending melt and oxidized into $CO_x$ gas is also plotted, for both the isentropic and the isothermal models). Fig. 1 indicates that only modest levels of coeruptive $CO_x$ gas suffice to launch small pyroclastic melt droplets at a $u$ greater than asteroidal $v_{esc}$. For example, in terms of the oxidative contribution of elemental C, ~2000 μg/g suffices to drive pyroclastic matter off an asteroid 200 km in diameter, 500 μg/g suffices for a diameter of 100 km, etc.

## 3. PYROCLAST SIZES

The basalt-removal process can be efficient only to the degree that the pyroclastic melt drops are consistently small. Fig. 1 assumes that the melt drops are launched at velocities very near the expansion velocity of the gas $u$. From gas-drag theory, the range of sizes over which this assumption is valid extends up to droplet diameter ($d$) ~2 mm (Wilson and Keil, 1997). Of course, if the blobs are big enough, they are not even propelled far enough to survive as discrete entities; they merge into, or simply erupt as, surface lava.

As discussed in this paper's Electronic Annex, the dominant sizes of liquid blobs produced during eruption of explosively gas-charged magmas are difficult to predict on theoretical grounds. To constrain the melt drop sizes, we can turn to analogs from the Moon and Io. The Moon, as a notoriously volatile-depleted body, might appear ill-suited as a progenitor of explosive volcanism. Nonetheless, pyroclastic melt (glass) droplets are a common ingredient of lunar regolith samples, and deposits of nearly pure pyroclastic glass, lunar equivalents of tuff, were sampled by both the Apollo-15 and Apollo-17 missions (Arndt and von Englehardt, 1987; Weitz et al., 1999). It is generally agreed that the volatile component of the lunar pyroclastic eruptions was almost exclusively $CO_x$ gas formed by oxidation of graphite entrained in the ascending magmas (Sato, 1979; Weitz et al., 1999). Graphite is an exception to the volatile-depletion trend, because it only becomes volatile, as fuel for generating $CO_x$ gas, in extremely limited circumstances (shallow/low-pressure and hot) within the lunar interior. But graphite's low density (2200 kg m$^{-3}$), combined with its frangibility, make it prone to entrainment. Only traces of graphite are found in the lunar megaregolith. Apparently, whatever graphite was entrained in the magma tended to be efficiently oxidized during the decompression as the hot magma rose to the surface. Individual lunar eruptive cycles produced remarkably restricted compositional ranges for their pyroclastic glasses (Delano, 1986). Including pyroclastic glasses scattered in the lunar regolith and thereby sampled at four additional Apollo landing sites (Shearer and Papike, 1993) as well as lunaite regolith breccias (Arai and Warren, 1999), many tens of discrete eruptive cycles appear to be represented. Among all of these different eruptions, the sizes of the pyroclasts were remarkably consistent, with $d$ usually within a factor of five of 100 μm (for details, see Electronic Annex).

For the silicate pyroclasts of two large-scale and long-lived eruptions on Io (not to be confused with the condensate "smoke" components of the same eruptive plumes), Cataldo et al. (2002) found that the thermal structures of the plumes suggest a "best mean diameter estimate" of close to 10 μm, although values as high as several hundred micrometers are not ruled out.

In summary, available constraints suggest that magmas erupting from within graphite-rich planetesimals generally develop large proportions of $CO_x$ gas, and that as the magma decompresses upon approach to the atmosphereless surface, the $CO_x$ bubbles grow so explosively that they disrupt the magma into pyroclastic droplets with $d$ generally smaller than 1 mm. The closest analogs, from the Moon, are typically ~0.1 mm in $d$. Droplets this small will be launched at velocities virtually as high as the expansion velocity of the gas, i.e., the $u$ of (2). They will also, as discussed in the next section, be prone to migrate inward toward the Sun as a consequence of Poynting–Robertson drag.

## 4. SMALL-BODY DRAG EFFECTS

The blow-off process, per se, can only displace the pyroclasts into orbits that are similar to that of the parent planetesimal. If these new orbits were to remain unmodified for several revolutions, the potential for reaccretion onto the parent planetesimal might be significant. However, objects with $d$ of order 0.001 to a few tens of mm spiral inward toward the Sun as a result of the Poynting–Robertson drag effect. This drag is a consequence of relativistic physics (Robertson, 1937), stemming from the disparity between absorption of light photons preferentially (as a result of aberration) into the leading side of the orbiting particle, versus isotropic emission of photons from the particle. Robertson derived an equation for the rate of infall assuming zero eccentricity $e$, and Wyatt and Whipple (1950) solved for the generic problem of the rate of infall for initial eccentricity $e_i$ between 0 and 0.99. A simplified form of equation (13) of Wyatt and Whipple (1950) is:

$$t_{P\text{-}R} = \tau d \rho a^2 \tag{5}$$

where $t_{P\text{-}R}$ is the duration of the infall to the Sun from initial semimajor axis $a$, $\rho$ is the particle's density, and $\tau$ is a complex function of $e_i$. For $t_{P\text{-}R}$, $d$ and $\rho$ in SI units (s, m and kg m$^{-3}$) and $a$ in AU, Wyatt and Whipple (1950) found that $\tau$ ranges from $1.11 \times 10^{13}$ s kg$^{-1}$ for $e_i = 0$, to $4.56 \times 10^{13}$ s kg$^{-1}$ for $e_i = 0.99$. For our purposes it is sufficient to note just a few $\tau$ results for intermediate $e_i$. For $e_i = 0.2$, $\tau$ is $1.64 \times 10^{13}$, and for $e_i = 0.4$, $\tau$ is $2.37 \times 10^{13}$ s kg$^{-1}$.

Fig. 2 shows the rate of Poynting–Robertson infall for spheroidal particles with $d$ between 0.01 and 1 mm, at distances from the Sun ($a$) of 0.6–2 AU, and $e_i$ of 0–0.4, calculated by numerical integration of results from (5). In interpreting Fig. 2, note that although the fastest $da/dt$ occurs at zero $e$, at nonzero $e$ the orbit is changing in shape

Author's personal copy



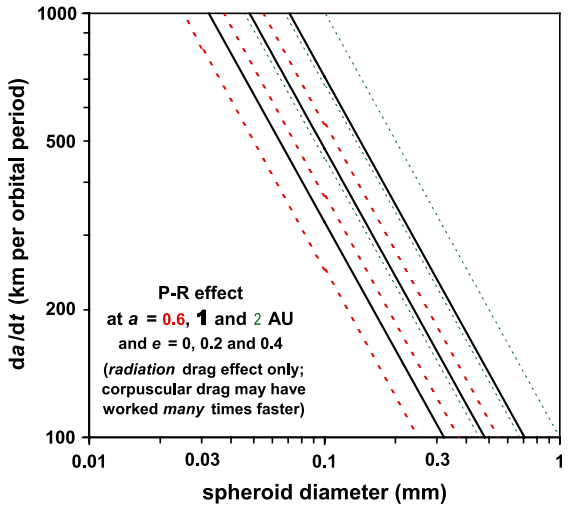


Fig. 2. Poynting–Robertson drag causes a rapid Sunward migration of the orbits of small solar-system objects such as pyroclastic materials blown off protoplanets. The diminution of semimajor axis $a$ is expressed here in terms of kilometers per orbital period. Dashed, solid and long-dashed curves represent the rate at 0.6, 1 and 2 AU, respectively. For each distance, a set of three curves is shown for eccentricity $e = 0$, 0.2 or 0.4 (fastest $da/dt$ occurs at $e = 0$). Curves shown ignore corpuscular (or "plasma-Poynting–Robertson") drag, which, depending on the early solar wind flux, may have worked many times faster for sweep-away of pyroclastic dusts (see text).

as well as distance from the Sun; so the effective, overall rate of displacement is faster than the high-$e$ curves in Fig. 2 might suggest. However, the rate of Poynting–Robertson infall is directly proportional to the Sun's luminosity, which was probably lower by a few tens of percent (Zahnle, 2006) at the time (roughly 5 Myr after formation of the Sun; Hevey and Sanders, 2006) when the first planetesimals underwent melting. Taking Fig. 2 at face value, for a plausible combination of conditions, $a \sim 1$ AU, $e \sim 0.2$, and $d \sim 0.2$ mm, the Poynting–Robertson effect moves pyroclasts inward toward the Sun by 250 km already in the first orbital period. For any $a > 0.6$ AU in combination with any $e < 0.4$, the Poynting–Robertson effect leads to displacement in $a$ by >100 km per orbital period for all $d < 0.24$ mm.

Another drag force, corpuscular drag (also called, among other terms, "solar-wind drag" or "plasma-Poynting–Robertson drag"), is often omitted from discussions on orbital evolution of small interplanetary particles, perhaps because its effect is a function of particle material properties. Available estimates (Mukai and Yamamoto, 1982; Ryabova, 2005) indicate that for small low-porosity silicate (obsidian) spheroids, corpuscular drag leads to an orbital spiral-in rate ~2.4 times faster than the rate from more familiar (radiation) Poynting–Robertson drag alone. Furthermore, the solar wind flux was probably far higher, conceivably several thousand times higher (Zahnle, 2006), at the time of early planetesimal melting.

The probability for reaccretion onto another proto-Earth-planetesimal would depend on the surface-area density of protoEarth-planetesimals within the zone of space through which spiral-in takes place, and the rate (duration) of the spiral-in through the zone. A "particle in the box" calculation after Wetherill (1967), assuming the zone is 0.5 AU wide and centered at 1 AU, and that the pyroclastic dust has $d \sim 0.1$ mm (and thus, assuming corpuscular drag ~3–10 times as effective as radiation Poynting–Robertson drag, the dust takes $\sim 10^4$ years to transit a zone half-width), suggests the reaccretion probability would be of order 1–10%, but possibly (depending on the assumed size distribution of the protoEarth-planetesimals) >>10%. Drag effects from conceivably surviving nebular gas (see above) would have a similarly size-dependent tendency to cause infall and separation of pyroclastic dusts from parent planetesimals (Cameron, 1995). Photophoresis (Krauss et al., 2007) represents yet another potential mechanism, if nebular gas survived, for the rapid removal of pyroclastic basalt dust.

## 5. REFERENCE QUANTITATIVE MODEL FOR EFFECTS OF BASALT DISSIPATION

Consider, as an end-member model, a scenario in which the first few percent of basaltic melt formed on the protoplanet is entirely lost by the pyroclastic blow-off mechanism. The trace-element compositions of the melt and the mantle residue during partial melting can be constrained by mass-balance equations (e.g., Zou, 2000, 2007). Two basic classes of models might be applied. One class assumes removal of melt from the source region occurs in one large batch (or in principle several batches; in older literature this batch model is sometimes confusingly termed "equilibrium" melting). Another class assumes that a continuous bleed-out of melt from the source region (Maaløe, 1982; Shaw, 2000); popularly termed either "continuous" or "dynamic" partial melting. Dynamic-melting models assume that the residuum's porosity $\Phi$ (the mass proportion of melt that persisting as interstitial melt within the residue) remains constant, i.e., bleed-out occurs at a critical melt-proportion (porosity) threshold. However, the trace-element characteristics of ureilites suggest that in at least one anatectic asteroid the style of melting was close to batch (Warren et al., 2006a).

As reviewed by Zou (2000, 2007), in nonmodal batch partial melting the concentration of a trace element in the melt $C_L$ is given by

$$C_L = \frac{C_0}{D_0 + f(1 - D_{nm})} \quad (6)$$

where $C_0$ is the initial bulk-system concentration (which will be consistently scaled to 1, for purposes of the present discussion), $D_0$ is the bulk modal solid/melt partition coefficient, $D_{nm}$ is the nonmodal melting solid/melt partition coefficient, and $f$ is the degree of melting, expressed in terms of mass fraction. Mathematically, $D_0 = \sum x^i K^i$ and $D_{nm} = \sum p^i K^i$, where $K^i$ is the crystal/melt partition coefficient for phase $i$, $x^i$ is the proportion of phase $i$ in the source rock, and $p^i$ is the proportion of phase $i$ in the matter contributing to the nascent melt. Conversion from $C_L$ to the composition of the bulk solids $C_S$ can be done using

Author's personal copy



$$D = \frac{D_0 - D_{\mathrm{nm}} f}{1 - f} \tag{7}$$

and the simple relationship

$$C_{\mathrm{S}} = DC_{\mathrm{L}} \tag{8}$$

For dynamic partial melting (Zou, 2000, 2007), the concentration of a trace element in the residual melt $C_f$ is given by

$$C_f = \frac{C_0}{D_0 + \Phi(1 - D_{\mathrm{nm}})}\left[1 - \frac{D_{\mathrm{nm}} + \Phi(1 - D_{\mathrm{nm}})}{D_0 + \Phi(1 - D_{\mathrm{nm}})} X\right]^{(1/[\Phi + (1-\Phi)D_{\mathrm{nm}}] - 1)} \tag{9}$$

where $X$ is the degree of melting, expressed in terms of mass fraction removed from the residue. The "critical" $\Phi$ at which permeable flow occurs is a complex and poorly understood function of the dihedral angle of crystal-melt juncture, which is high (conducive to melt connectivity) for olivine, so that in olivine-dominated anatectic materials $\Phi$ is usually assumed to be of order 0.001–0.02 (Sims et al., 1999; Bourdon et al., 2006). Possibly in the low gravity environment of planetesimals, especially planetesimals with high pyroxene/olivine ratios, $\Phi$ is systematically higher.

The relationship between $X$ and the more commonly envisaged total mass proportion of melt $f$ is given by $f = \Phi(1 - X) + X$; or $X = 1 - (1 - f)/(1 - \Phi)$. As long as $X$ is not $>>0.1$, to a rough approximation $f \sim \Phi + X$. The concentration in the residual solid is

$$C_{\mathrm{s}} = D_{\mathrm{d}} C_{\mathrm{f}} \tag{10}$$

where the dynamic bulk distribution coefficient $D_{\mathrm{d}}$ is given by

$$D_{\mathrm{d}} = \frac{D_0 - D_{\mathrm{m}}[X + \Phi(1 - X)]}{(1 - X)(1 - \Phi)} \tag{11}$$

Most pertinent for present purposes is

$$C_{\mathrm{res}} = \Phi C_{\mathrm{f}} + (1 - \Phi) C_{\mathrm{s}} \tag{12}$$

where $C_{\mathrm{res}}$ is the concentration in the total (solid plus is residual melt) residue. Total residue concentrations can also be calculated for a batch-melting model in which a finite proportion of melt ($\Phi$) is left behind, by trivial modification of (8). At the theoretical limit of $\Phi$ going to 0, dynamic melting becomes "fractional fusion."

Crystal/melt distribution coefficients ($K$) for REE and minerals potentially important during planetesimal anatexis are listed in Table 1. The $K$ values for Eu are profoundly influenced by oxygen fugacity. Extremely low $fO_2$ changes this element's valency from 3+ to 2+, while other REE remain trivalent. By analogy with ureilites (Warren and Kallemeyn, 1992, Fig. 6), anatexis with stable graphite (before entrainment in surface-approaching magma), FeNi-metal, and magnesian (roughly $Fo_{88}$) olivine, implies $fO_2$ was certainly below $10^{-13}$ atm and most likely, assuming the temperature $T$ of melting was ~1200 °C, close to $10^{-14}$ atm (cf. Fogel, 2005).

Most importantly, for plagioclase (plag) at low $fO_2$, $K$ is vastly higher for Eu than for other REE. Two sets of experiments have constrained this effect. McKay (as reviewed in McKay, 1989) found a trend in which $K_{\mathrm{Eu}}$ is roughly proportional to $-\log(fO_2)$ until, as $fO_2$ falls much below $10^{-10}$ atm, the trend starts to level off, and the $K$ value approaches that of $Eu^{2+}$, which is 1.25. The $K_{\mathrm{Eu}}$ implied by this trend at $-\log(fO_2) = 14$ would be 1.13. However, these experiments were not ideally suited for our purpose, because they were based on low-Na/Ca systems (lunar analogs, primarily), whereas the scenario we seek to model probably involved highly albitic plag, based on chondrite data (e.g., Fredriksson et al., 1975; Dube et al., 1977; Hutchison et al., 1981); and on the plagioclases found (rarely) in ureilites, mostly $An_{15}$ or less (Kita et al., 2004; Warren et al., 2006b). Sun et al. (1974) reported a series of experiments with similarly basaltic system compositions except more albitic ($An_{69}$) plag. In their formulation, $K_{\mathrm{Eu}}$ is, at any given $T$, directly proportional to $-\log(fO_2)$; and the value of $K_{\mathrm{Eu}}$ at $fO_2 \sim 10^{-14}$ atm and ~1200 °C is 0.70. It is hard to assess which of these alternative $K_{\mathrm{Eu}}$ values is the more reliably applicable. In principle, the more albitic data set (Sun et al., 1974) is more relevant; and extrapolation to a more albitic system would imply a $K_{\mathrm{Eu}}$ even lower than 0.7. However, only McKay's data set is based on several discrete experiments conducted over a span of years. For purposes of modeling, values of both 0.7 and 1.1 have been tested.

While extremely low $fO_2$ engenders an anomalously high-$K_{\mathrm{Eu}}$ for plag, it has the opposite effect on most other minerals. For olivine and pigeonite, the low-$K_{\mathrm{Eu}}$ values are direct from the same low-$fO_2$-oriented sources used for the other REE (Kennedy et al., 1993; McKay et al., 1986, 1991). However, for some $K$ values the $fO_2$ effect had to be extrapolated. The value for high-Ca pyroxene is extrapolated from the large Eu anomalies in ureilite augites,

Table 1
Crystal/melt partition coefficients adopted for use in trace element modeling

| | La | Ce | Nd | Sm | Eu | Gd | Yb | Lu | Hf | Source (for trivalent REE) |
|---|---|---|---|---|---|---|---|---|---|---|
| Olivine | 0.00003 | 0.00007 | 0.00003 | 0.0009 | 0.0005 | 0.0011 | 0.024 | 0.030 | 0.011 | Kennedy et al. (1993) |
| Opaque oxides | 0.01 | 0.01 | 0.01 | 0.02 | 0.01 | 0.03 | 0.04 | 0.04 | 0.30 | Various literature |
| Orthopyroxene | 0.0004 | 0.0011 | 0.006 | 0.021 | [0.005] | 0.052 | 0.270 | 0.300 | 0.012 | Lee et al. (2007) |
| Plagioclase | 0.041 | 0.036 | 0.027 | 0.021 | 0.7–1.1 | 0.015 | 0.0049 | 0.0041 | 0.0034 | McKay (1989) |
| High-Ca pyroxene | 0.032 | 0.064 | 0.149 | 0.254 | [0.03] | 0.35 | 0.40 | 0.38 | 0.24 | Norman et al. (2005) |
| Pigeonite ($Wo_{10}$) | 0.0015 | 0.0036 | 0.014 | 0.024 | 0.012 | 0.041 | 0.157 | 0.157 | 0.030 | McKay et al. (1986, 1991) |

Eu values in squared brackets are extrapolations (see text) from Eu/Eu* in ureilites (high-Ca pyroxene: Guan and Crozaz, 2000, 2001), or Eu/Eu* in acapulcoites and lodranites (orthopyroxene: Floss, 2000).

Other sources: All Hf values are adopted after Beard et al. (1998). Caveat: these Hf values seems especially uncertain (cf., for example, Kennedy et al., 1993). Regarding Eu in plag, see text.

Author's personal copy



which are about three times more strongly negative than the anomalies in ureilitic pigeonites (Guan and Crozaz, 2000, 2001). The extrapolation of $K_{Eu}$ for orthopyroxene (opx) is based on analogous data for different pyroxenes in acapulcoites and lodranites, a suite of primitive (near-chondritic) restitic a chondrites distinct from the ureilites (Floss, 2000). The Eu anomaly among the $K_{REE}$ for the inconsequential opaque-oxide component is based mainly on Nakamura et al. (1986).

Even the lightest REE, La, is not the most incompatible of all elements. For purposes of representing an almost totally incompatible element, most models include Th. $K_{Th}$ is assumed equal to 0.0001 for all phases except olivine, for which $K_{Th}$ is assumed $= K_{La}$ (Table 1).

As a preliminary reference model, the initial source phase proportions are assumed to be 50 wt% olivine, 39 wt% pyroxene, 10 wt% plag and 1 wt% opaque oxides. Here, the olivine/pyroxene ratio has been selected to approximately match the CIPW norm for an average of literature estimates (Warren, 2005) for the composition for Earth's "primitive mantle," which implies a fictive 51 wt% olivine, 30 wt% opx ($Wo_0$) and 5 wt% high-Ca pyroxene ($Wo_{50}$), along with 12 wt% plag and 1 wt% opaque oxides. Another consideration is that among chondritic materials, there is a tendency for pyroxene/olivine ratio to be high if the MgO/FeO ratio is high (i.e., a large proportion of the iron is reduced Fe instead of FeO: Mueller and Olsen, 1967). Compared to most types of chondrites (e.g., Jarosewich, 1990), the Earth not only has a high MgO/FeO, but also an extremely high proportion of reduced Fe (the FeNi-dominated core constitutes 31.5 wt% of the Earth), matched (approximately) only by a single type of chondrite, EH-enstatite, which is essentially devoid of olivine. If Javoy (1995, 1999) is to any extent correct in arguing that the bulk Earth accreted mainly from matter similar to enstatite chondrites (cf. Wasson, 1977), with the final FeO content raised by late accretion of oxidizing matter and/or high-pressure reduction of $SiO_2$ to (core) Si-metal, then the olivine/pyroxene ratio of the averaged conventional "primitive mantle" estimate should be viewed as an upper limit for our purposes. Javoy (1995, 1999) EH chondrite model is an extreme end-member interpretation, but to allow for the general scenario of a comparatively "reduced" starting material, many of the models tested assume an intermediate composition, with initial source phase proportions of 30 wt% olivine, 59 wt% pyroxene, 10 wt% plag and 1 wt% opaque oxides. An additional minor consideration is that the basalt dissipation process we seek to model implies that the final Earth has lost several wt% of pyroxene, but no olivine, relative to the original starting matter.

The bulk-Earth abundance of $Al_2O_3$ (which effectively determines CIPW plag) is not well known (Javoy, 1999; Lyubetskaya and Korenaga, 2007), and the 12 wt% plag implied by the CIPW calculation ignores the tendency for a significant proportion of $Al_2O_3$ to reside in pyroxene. Modes for highly equilibrated chondrites typically have ~10 wt% plag; and also opx/(total pyroxene) ratio ~0.8 (Fredriksson et al., 1975; Dube et al., 1977). The reference model thus assumes 10 wt% plag and that the pyroxene is 4/5 (by weight) opx, 1/5 high-Ca pyroxene. Pigeonite has been included in Table 1 and in some tested models; with the ratio opx/(opx + augite), for the remaining pyroxene, fixed at 0.8. However, among mafic igneous systems, as *mg* increases toward the high values appropriate for Earth protoplanets, pigeonite is increasingly unstable versus combinations of opx and high-Ca pyroxene (Longhi and Pan, 1988).

For determination of the nonmodal melting partition coefficient $D_{nm}$ in the reference model, the matter contributing to the melt is assumed to be a 60:40 (by weight) mix of plag and pyroxene, with proportionality among the pyroxene types remaining the same in the residuum as in the initial matter. As reviewed by Fogel (2005), the plag/pyroxene ratio of the melting matter will be sensitive to the Na/Ca ratio in the bulk material, and secondarily to the ratio MgO/FeO. Typical planetary basalts have low-moderate Na/Ca and moderate *mg*, and consequently slightly more pyroxene than plag. However, the relatively high Na/Ca ratios typical of primitive chondrites, and of the plagioclases found in (polymict) ureilites (Goodrich et al., 2004; Warren et al., 2006b), cause the cotectic between pyroxene and plag to shift in the direction of higher plag/pyroxene melting ratio. Admittedly, this important effect has never been very systematically constrained by experimental petrology, but based on the constraints that are available (see Fogel, 2005), 0.6 seems a conservatively low choice for the melt-entering plag/(plag + pyroxene) ratio.

In a real-world accretion sequence, the planet would probably grow from protoplanets with a wide variety of extents of basalt loss. However, to keep the modeling tractable, and results comprehensible, we will assume that each model Earth forms from just two classes of protoplanets: one class that has undergone a uniform extent of basalt loss, and another class that has undergone absolutely no basalt loss. One of the most important parameters in the models is thus the mass proportion $Y$ of the final Earth that is assumed to accrete from unfractionated matter (the proportion that derives from basalt-dissipated protoplanets is simply $1 - Y$). The initial composition of the component that undergoes basalt loss is assumed identical to that of the unfractionated $Y$ component. As another modeling simplification, all loss of basalt is limited to the earliest stages of melt segregation from the mantle, i.e., a single, initial batch of melt in the batch model, or all melt erupted from the inception of melt extraction up to some plausible $X$ in the dynamic-melting model.

## 6. MODEL RESULTS

The scenario of explosive-volcanic basalt dissipation on putative Earth protoplanets is too uncertain, in terms of the overall efficiency of basalt loss, and also in terms of the stage(s) in the progressive melting history of the protoplanet at which basalt blow-off occurs, for geochemical modeling to establish any tight constraint on the final-Earth Nd/Sm. However, modeling can also serve to constrain (not tightly, but usefully) the pattern of final-Earth depletions in other geochemical ratios, such as Al/Ca and Hf/Lu, implied to accompany any given final-Earth Nd/Sm.

Author's personal copy



The magnitude of the Eu anomaly figures as an important aspect of the modeling. To simplify discussion, I will cite the Eu anomaly in terms of Eu/Eu*, where (after Brophy and Basu, 1990) Eu* is the Eu concentration implied by interpolation between the adjacent REE, Sm and Gd (such that the Sm, Eu* and Gd concentrations are linear on a plot of atomic number versus log CI-normalized concentration). In discussing model results, the Eu of this Eu/Eu* will, unless otherwise noted, refer to a Eu concentration modeled based on $K_{Eu,plag} = 0.7$.

Among the various models tested (Tables 2 and 3; also Annex Tables EA-1 and EA-2) there is little or no correlation between the $X$ at which Eu/Eu* passes through unity and final-Earth Nd/Sm. But as a useful measure of model success, and to facilitate comparison among models that otherwise would require detailed illustration, we will focus on the final-Earth Nd/Sm ratio under conditions where the final-Earth Eu anomaly is negligible. As will be seen, this approach introduces a bias against extreme values of $X$ (values between ~3 and 14 wt% are favored), but the same bias against extreme $X$ may exist in nature. If short-lived $^{26}$Al is a major heat source, then heating will likely continue until melting has removed a large fraction of the initial plag, i.e., heat-generating Al. The ureilites, admittedly, lost virtually all of their plag, but this appears to have resulted from a distinctive collisional history (Warren and Kallemeyn, 1992; Goodrich et al., 2004; Warren et al., 2006a,b), not shared by, for example, the lodranite parent body (Mittlefehldt et al., 1998; Floss, 2000).

Henceforward the lowest final-Earth Nd/Sm ratio that is implied by any given model sequence of planetesimal basalt loss, with the further constraint that the final-Earth Eu/Eu* must be within 1% of 1, will be designated $(Nd/Sm)_Y$. The subscript $Y$ (or more commonly, a value assumed for $Y$) is part of the designation, because final-Earth Nd/Sm is always sensitive to the magnitude of the unfractionated ($Y$) component. Thus, for example, "$(Nd/Sm)_{0.60}$" represents the lowest final-Earth Nd/Sm ratio that results, while the final-Earth Eu/Eu* (based on $K_{Eu,plag} = 0.7$) is between 0.99 and 1.01, in any given model of planetesimal melting and basalt loss, assuming the final Earth is a mixture of 60 wt% unfractionated matter with 40 wt% basalt-depleted planetesimals. The choice of 1% as the reference "margin of error" for the final-Earth Eu/Eu* is obviously arbitrary, but 1% makes for easy interpolation, and would be very difficult to detect in estimations of the real bulk-Earth composition.

As will be seen, models predicated on dynamic melting tend to deplete incompatible trace elements at relatively low $f$ (for any given assumed $\Phi$) in comparison to batch-melting models. An indirect consequence is that similar results, in terms of final-Earth composition, are obtained assuming a higher residue porosity $\Phi$ but a slightly smaller unfractionated component $Y$ in dynamic-melting models in contrast to batch-melting models. Thus, in the discussion below the $Y$ value used for a (necessarily small) set of models used for inter-model comparisons is lower (0.55) for dynamic-melting models than the $Y(0.60)$ used for batch-melting models.

Table 2
Results from a selection of batch-melting based models (for a more complete selection see Table EA-1)

| Entering-melt plag | Initial fraction | | | Melt | Residual | Melt | Mixing | Final-Earth composition | | | | | | | | | |
|---|---|---|---|---|---|---|---|---|---|---|---|---|---|---|---|---|---|
| | Olvn | Pigeon | Plag | $f$ | $\theta$ | $X$ | $Y$ | Tn | Hf | La | Nd | Sm | Eu | Gd | Lu | Nd/Sm | Eu/Eu* | Eu[a]/Eu* | Al/Ca |
| 0.6 | 0.5 | 0 | 0.10 | 0.094 | 0.005 | 0.089 | 0.50 | 0.529 | 0.650 | 0.550 | 0.593 | 0.638 | 0.668 | 0.686 | 0.827 | 0.929 | 1.010 | 1.079 | 0.814 |
| 0.6 | 0.5 | 0 | 0.10 | 0.091 | 0.005 | 0.086 | 0.60 | 0.624 | 0.723 | 0.641 | 0.676 | 0.713 | 0.739 | 0.751 | 0.865 | 0.949 | 1.010 | 1.061 | 0.858 |
| 0.6 | 0.5 | 0 | 0.10 | 0.088 | 0.005 | 0.083 | 0.70 | 0.719 | 0.795 | 0.732 | 0.759 | 0.787 | 0.810 | 0.816 | 0.901 | 0.964 | 1.010 | 1.046 | 0.900 |
| 0.6 | 0.5 | 0 | 0.10 | 0.090 | 0.03 | 0.061 | 0.50 | 0.669 | 0.757 | 0.685 | 0.716 | 0.749 | 0.773 | 0.782 | 0.882 | 0.957 | 1.010 | 1.053 | 0.877 |
| 0.6 | 0.5 | 0 | 0.10 | 0.086 | 0.03 | 0.058 | 0.60 | 0.741 | 0.812 | 0.754 | 0.779 | 0.805 | 0.827 | 0.832 | 0.910 | 0.968 | 1.010 | 1.043 | 0.909 |
| 0.6 | 0.5 | 0 | 0.10 | 0.080 | 0.03 | 0.052 | 0.70 | 0.814 | 0.867 | 0.824 | 0.843 | 0.862 | 0.881 | 0.882 | 0.938 | 0.977 | 1.010 | 1.033 | 0.941 |
| 0.6 | 0.3 | 0 | 0.10 | 0.051 | 0.005 | 0.046 | 0.50 | 0.555 | 0.756 | 0.605 | 0.691 | 0.759 | 0.795 | 0.816 | 0.924 | 0.910 | 1.010 | 1.070 | 0.911 |
| 0.6 | 0.3 | 0 | 0.10 | 0.048 | 0.005 | 0.043 | 0.60 | 0.647 | 0.813 | 0.690 | 0.761 | 0.815 | 0.845 | 0.860 | 0.943 | 0.933 | 1.010 | 1.054 | 0.935 |
| 0.6 | 0.3 | 0 | 0.10 | 0.041 | 0.005 | 0.036 | 0.70 | 0.741 | 0.872 | 0.777 | 0.833 | 0.874 | 0.898 | 0.906 | 0.963 | 0.953 | 1.010 | 1.039 | 0.960 |
| 0.6 | 0.3 | 0 | 0.10 | 0.073 | 0.03 | 0.044 | 0.50 | 0.709 | 0.816 | 0.731 | 0.777 | 0.818 | 0.828 | 0.854 | 0.934 | 0.951 | 0.990 | 1.028 | 0.916 |
| 0.6 | 0.3 | 0 | 0.10 | 0.076 | 0.03 | 0.047 | 0.60 | 0.760 | 0.846 | 0.777 | 0.815 | 0.847 | 0.854 | 0.878 | 0.944 | 0.961 | 0.990 | 1.020 | 0.927 |
| 0.6 | 0.3 | 0 | 0.10 | 0.081 | 0.03 | 0.053 | 0.70 | 0.813 | 0.877 | 0.825 | 0.853 | 0.878 | 0.881 | 0.902 | 0.954 | 0.972 | 0.990 | 1.012 | 0.939 |

[a] The model final-Earth Eu result assuming $K_{Eu}$ for plag = 1.1 (instead of 0.7). CAVEAT: results shown have been arbitrarily selected, in terms of $f$ (or $X$), to have Eu/Eu* ~1. As one indication of the actual uncertainty in Eu/Eu*, note that this criterion leads to Eu[a]/Eu* being consistently >1.

Author's personal copy



Table 3
Results from a selection of dynamic-melting based models (for a more complete selection see Table EA-2)

| Entering-melt plag | Initial fraction | | | Melt | Residual | Melt | Mixing | Final-Earth composition | | | | | | | | | | |
|---|---|---|---|---|---|---|---|---|---|---|---|---|---|---|---|---|---|---|
| | Olvn | Pigeon | Plag | $f$ | $\theta$ | $X$ | $Y$ | Tn | Hf | La | Nd | Sm | Eu | Gd | Lu | Nd/Sm | Eu/Eu$^*$ | Eu$^a$/Eu$^*$ | Al/Ca |
| 0.6 | 0.5 | 0 | 0.10 | 0.123 | 0.005 | 0.119 | 0.50 | 0.500. | 0.506 | 0.500 | 0.501 | 0.511 | 0.530 | 0.540 | 0.705 | 0.980 | 1.010 | 1.072 | 0.747 |
| 0.6 | 0.5 | 0 | 0.10 | 0.120 | 0.005 | 0.116 | 0.60 | 0.600. | 0.605 | 0.600 | 0.601 | 0.610 | 0.628 | 0.634 | 0.768 | 0.985 | 1.010 | 1.056 | 0.807 |
| 0.6 | 0.5 | 0 | 0.10 | 0.116 | 0.005 | 0.111 | 0.70 | 0.700. | 0.705 | 0.700 | 0.701 | 0.709 | 0.725 | 0.728 | 0.830 | 0.989 | 1.010 | 1.044 | 0.863 |
| 0.6 | 0.5 | 0 | 0.10 | 0.117 | 0.03 | 0.090 | 0.50 | 0.505 | 0.585 | 0.536 | 0.564 | 0.600 | 0.627 | 0.642 | 0.778 | 0.941 | 1.010 | 1.066 | 0.812 |
| 0.6 | 0.5 | 0 | 0.10 | 0.114 | 0.03 | 0.086 | 0.60 | 0.605 | 0.674 | 0.633 | 0.656 | 0.685 | 0.709 | 0.719 | 0.828 | 0.957 | 1.010 | 1.051 | 0.859 |
| 0.6 | 0.5 | 0 | 0.10 | 0.108 | 0.03 | 0.080 | 0.70 | 0.706 | 0.763 | 0.729 | 0.749 | 0.772 | 0.792 | 0.798 | 0.878 | 0.970 | 1.010 | 1.039 | 0.904 |
| 0.6 | 0.3 | 0 | 0.10 | 0.080 | 0.005 | 0.075 | 0.50 | 0.500 | 0.574 | 0.501 | 0.530 | 0.596 | 0.638 | 0.671 | 0.838 | 0.890 | 1.010 | 1.112 | 0.845 |
| 0.6 | 0.3 | 0 | 0.10 | 0.077 | 0.005 | 0.072 | 0.60 | 0.600 | 0.665 | 0.601 | 0.627 | 0.682 | 0.719 | 0.743 | 0.875 | 0.920 | 1.010 | 1.083 | 0.884 |
| 0.6 | 0.3 | 0 | 0.10 | 0.072 | 0.005 | 0.067 | 0.70 | 0.700 | 0.756 | 0.701 | 0.725 | 0.769 | 0.800 | 0.816 | 0.912 | 0.943 | 1.010 | 1.060 | 0.921 |
| 0.6 | 0.3 | 0 | 0.10 | 0.082 | 0.03 | 0.053 | 0.50 | 0.549 | 0.712 | 0.617 | 0.678 | 0.732 | 0.749 | 0.782 | 0.883 | 0.925 | 0.990 | 1.041 | 0.895 |
| 0.6 | 0.3 | 0 | 0.10 | 0.086 | 0.03 | 0.057 | 0.60 | 0.632 | 0.759 | 0.683 | 0.731 | 0.776 | 0.788 | 0.816 | 0.901 | 0.943 | 0.990 | 1.029 | 0.910 |
| 0.6 | 0.3 | 0 | 0.10 | 0.092 | 0.03 | 0.064 | 0.70 | 0.717 | 0.807 | 0.752 | 0.787 | 0.820 | 0.828 | 0.852 | 0.919 | 0.960 | 0.990 | 1.018 | 0.925 |

[a] The model final-Earth Eu result assuming $K_{Eu}$ for plag = 1.1 (instead of 0.7). CAVEAT: results shown have been arbitrarily selected, in terms of $f$ (or $X$), to have Eu/Eu$^*$ ~1. As one indication of the actual uncertainty in Eu/Eu$^*$, note that this criterion leads to Eu$^a$/Eu$^*$ being consistently >1.

### 6.1. Batch-melting

Figs. 3 and 4 illustrate a range of scenarios for depletion of protoplanets, and eventually the Earth, by dissipative loss of batch-segregated partial melts. In batch-melting scenarios, the final-Earth's Nd/Sm at first declines as $f$ increases from 0 to a few percent above $\Phi$. But with further increase in $f$, even though the planetesimal residuum's Nd/Sm continues to decline, the final-Earth's Nd/Sm either levels off (in high-$\Phi$ models) or slowly rises back toward unity, as the residuum concentrations of Nd and Sm become so low that they contribute less and less to the final-Earth composition. A problem with most batch-melting scenarios, particularly if $K_{Eu,plag}$ is assumed to be 1.1, is that at low $f$ plag imparts a strongly positive Eu anomaly to the residuum; until roughly half of the plag is consumed (total exhaustion of plag, starting from initially 10 wt%, occurs at $f = 0.1667$), Eu is not even as depleted as Gd. Complete reduction of the Eu anomaly (Eu/Eu$^* = 1$) does not occur until the Eu curve declines to about mid-way between the Sm and Gd curves; e.g., in the case of Fig. 3a at $f \sim 0.10$, and $(Nd/Sm)_{0.60} = 0.949$. The Nd/Sm minimum in a model identical in all respects except initial pyroxene/olivine ratio (Fig. 3c) comes at $f \sim 0.06$, and $(Nd/Sm)_{0.60} = 0.932$. Of course, the batch-melting model is predicated on an assumption that melt segregation is enabled only at high-moderate $f$ (facile segregation of melt at low $f$ is the defining characteristic of dynamic melting).

The heavy-discontinuous curves in Fig. 3 illustrate the disadvantage, from a strictly Nd/Sm standpoint, of a higher proportion of unfractionated matter $Y$ in the final-Earth mixture. However, as discussed in Section 6.5, a low $Y$ has the potentially problematic effect of enhancing, in the final Earth, interelement fractionations in general, including between thoroughly incompatible elements (e.g., Th and La) and more compatible elements, and between the major oxides $Al_2O_3$ and CaO.

The incompatible element patterns that result from three of the same batch-melting scenarios are illustrated in Fig. 4. For the final Earth, these three batch-melting REE patterns are broadly similar to one another.

### 6.2. Dynamic melting

Fig. 5 and Annex Fig. EA-1 illustrate a range of scenarios predicated on dynamic (continuous-percolation) partial melting. In dynamic melting scenarios, the final-Earth's Nd/Sm at first steeply declines to very low levels as $f$ increases to a few percent more than $\Phi$. Compared to a batch-melting scenario (Fig. 3), the minimum in the final-Earth Nd/Sm trend is considerably lower, but the trend's rise back toward unity, as the residuum concentrations of Nd and Sm become less important, is also steeper; and thus Nd/Sm values at high $f$ are not very different from the values at high $f$ of batch-melting scenarios. The rise in the final-Earth Nd/Sm curve back toward 1, after its minimum, is less steep if $\Phi$ is high (contrast Fig. 5a versus b, or c versus d). The REE pattern has a substantial positive Eu anomaly (the depletion of Eu is comparable to that of Gd) until $f$ is well past the value of the final-Earth Nd/Sm

Author's personal copy



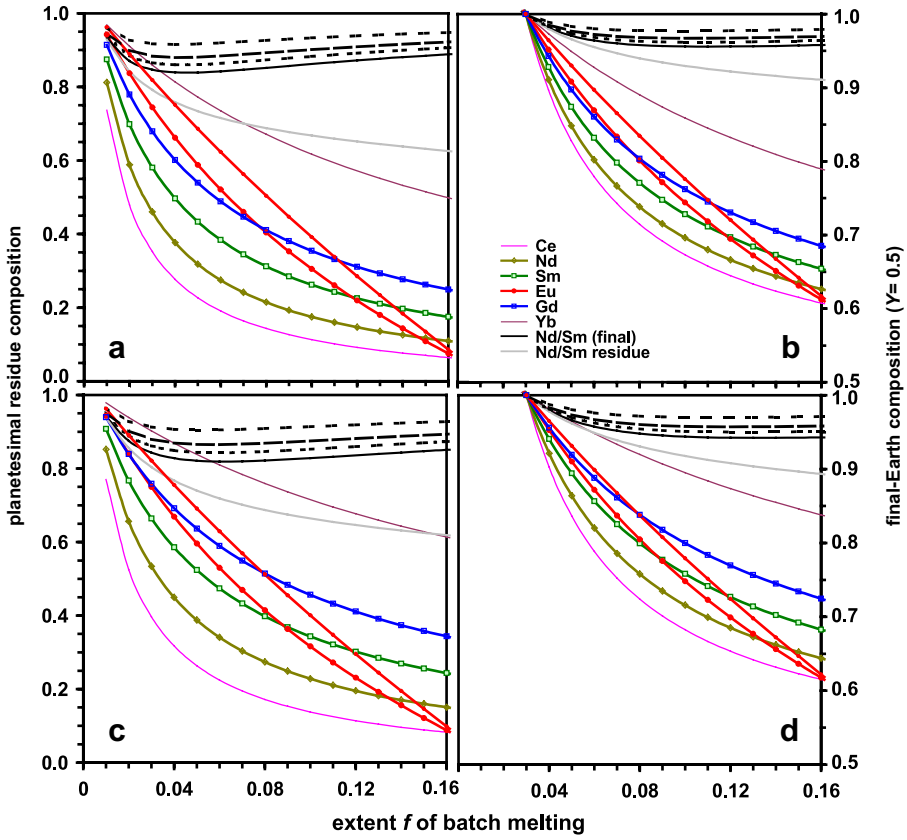


Fig. 3. Mantle residuum (solid plus residual melt) composition for an Earth protoplanet, calculated after Zou (2000, 2007) as a function of $f$ in a nonmodal batch-melting model. In each case, right-side scale shows the residuum concentrations of the left-side scale translated into final-Earth concentrations, assuming unfractionated component $Y = 0.50$. In (a) and (b), initial mineral assemblage is assumed to include 50 wt% olivine and 39 wt% pyroxene, whereas (c) and (d) assume 30 wt% olivine and 59 wt% pyroxene. Residual melt porosity after batch-melt removal is assumed 0.5 wt% for (a) and (c), 3 wt% for (b) and (d). Otherwise, all model parameters conform to the reference model described in the text. Heavy black dashed curves indicate effects of different choices of $Y$ (0.50, 0.55, 0.60 and 0.65) on final-Earth Sm/Nd (the scale for which is on the right side of the diagram). In each case, two concentration curves are shown for Eu. Leftward curve (with noticeably large filled-circle symbols) assumes $K_{Eu,plag} = 0.7$; rightward curve assumes $K_{Eu,plag} = 1.1$.

minimum. The $(Nd/Sm)_{0.55}$ results for Fig. 5b, c and d are 0.950, 0.906 and 0.934, respectively, and the minima on the final-Earth Nd/Sm curves occur at $f \sim 0.09$, 0.05, and 0.10, respectively. Note, however, that the $f$ of these minima and the $f$ of the $(Nd/Sm)_Y$ (which further require that $Eu/Eu^* = 0.99 - 1.01$) are not identical, or even necessarily close. Also, the magnitude of the lost basalt component is less than the $f$ values plotted in Fig. 5 by approximately $\Phi$ (i.e., in the case of Fig. 5b or d, by ~0.03). Again, the heavy-discontinuous curves in Fig. 5 illustrate the disadvantage, from a strictly Nd/Sm standpoint, of a higher proportion of unfractionated matter $Y$ in the final-Earth mixture.

The incompatible element patterns that result from three of the same dynamic melting scenarios are illustrated in Fig. EA-1. Elements more incompatible than Sm are so efficiently removed from the depleted planetesimal in low-$\Phi$ dynamic-melting models (such as Fig. 5c) that the final-Earth REE pattern is distinctively angular: nearly flat from La through Nd, yet showing approximately the same slope as the Fig. 4 patterns for Nd through Lu.

### 6.3. Major oxides: $Al_2O_3$ and CaO

Loss of basalt from Earth protoplanets will also deplete two of the major oxides, CaO and especially $Al_2O_3$. These depletions can be estimated by simple application of stoichiometry (see Electronic Annex). Results for $Al_2O_3$ and Al/Ca ratio are shown in Fig. 6, assuming the melting pyroxene was $En_{65}Wo_{10}$ with 0.5 wt% $Al_2O_3$, and treating melting-plag An, $X$ and $Y$ all as independent variables. The initial matter is assumed to be an average of various chondrite types (using primarily the data compilations of Wasson and Kallemeyn, 1988; Jarosewich, 1990). Conservatively ignoring the dilution (in some chondrite types) of the silicates by metal, but excluding the extremely volatile-rich CI, the average initial matter is thus modeled as containing 2.39 wt% $Al_2O_3$ and 1.93 wt% CaO. Models that combine high $f$ with low $Y$ imply considerable depletion of $Al_2O_3$, and to a lesser extent Al/Ca, relative to the initial material. Among the model results, depletion of Al/Ca is, for all practical purposes, precisely in proportion to the depletion of $Al_2O_3$. Assuming the melting plagioclase was

Author's personal copy



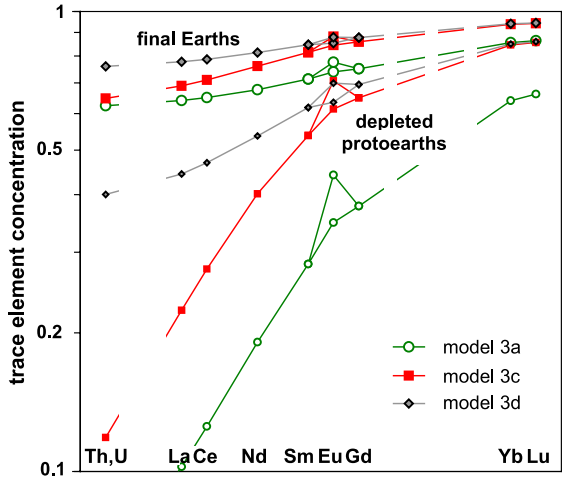


Fig. 4. Depletion patterns for REE and Th in three of the same batch-melting scenarios shown in Fig. 3. Variants shown assume unfractionated component $Y = 0.6$, along with an $f$ that gives $Eu/Eu^* \approx 1$. Final-Earth Nd/Sm is 0.949, 0.933 and 0.961 in models 3a, 3c and 3d, respectively. Curves are shown for $K_{Eu,plag}$ being both 0.7 and 1.1. For analogous diagram based on dynamic melting, cf. Fig. EA-1.

roughly $An_{25}$, any cited $(Al/Ca)_Y$ result may be converted to an $Al_2O_3$ result using $Al_2O_3 = 1.32(Al/Ca) - 0.33$.

### 6.4. The ureilite analogy quantified

The ureilites are imperfect analogs, and not just because they mostly have far lower *mg* than likely prevailed among Earth-progenitor materials. As reviewed by Guan and Crozaz (2000), the ureilites ended up completely purged of residual melt; and consequently their incompatible-element depletions are so extreme that most analyses (especially for light REE) suffer from terrestrial contamination. This contamination problem renders it impossible to estimate, for light REE, an average ureilite composition. Unfortunately, other restitic-mantle meteorites are even less suitable for analog purposes. Aubrites are so extremely reduced that sulfides, not silicates, acted as the major REE host (Mittlefehldt et al., 1998). Also, both aubrites and lodranites are so extremely coarse-grained that representative bulk sampling is impossible (Mittlefehldt et al., 1998; Floss, 2000).

To circumvent the contamination problem, some ureilite analyses have been conducted after leaching with acid.

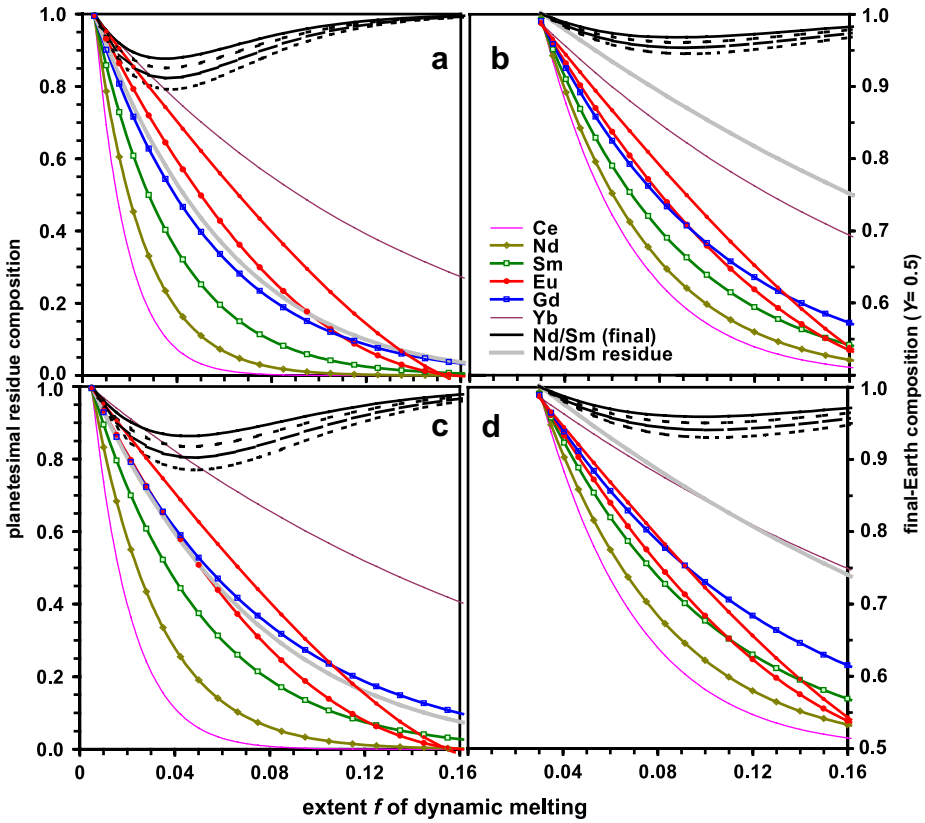


Fig. 5. Mantle residuum (solid plus residual melt) composition for an Earth protoplanet, calculated after Zou (2000, 2007) as a function of $f$ in a nonmodal dynamic-melting model. In each case, right-side scale shows the residuum concentrations of the left-side scale translated into final-Earth concentrations, assuming unfractionated component $Y = 0.50$. In (a) and (b), initial mineral assemblage is assumed to include 50 wt% olivine and 39 wt% pyroxene, whereas (c) and (d) assume 30 wt% olivine and 59 wt% pyroxene. Residual melt porosity during melt removal is assumed 0.5 wt% for (a) and (c), 3 wt% for (b) and (d). Otherwise, all model parameters conform to the reference model described in the text. Heavy black dashed curves indicate effects of different choices of $Y$ (0.50, 0.55, 0.60 and 0.65) on final-Earth Sm/Nd (the scale for which is on the right side of the diagram). In each case, two concentration curves are shown for Eu. Leftward curve (with noticeably large filled-circle symbols) assumes $K_{Eu,plag} = 0.7$; rightward curve assumes $K_{Eu,plag} = 1.1$.

Author's personal copy



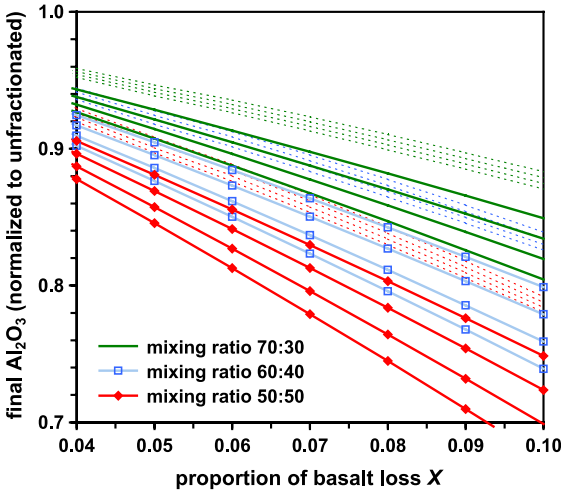


Fig. 6. Final-Earth depletion of $Al_2O_3$ shown as a function of the proportion of basalt lost $X$ with three different values assumed for $Y$ (0.5, 0.6 and 0.7), and for each of these, four different assumed compositions for the plag that is entering the melt (in order of increasing implied depletion: $An_{10}$, $An_{20}$, $An_{30}$ and $An_{40}$). Other model assumptions are discussed in the text. Also shown (light-dashed curves) is the narrower range of corresponding depletions in the Al/Ca (weight) ratio.

Fig. 7 shows one case, which happens to be an extraordinarily high-*mg* ureilite (ALH82130), where an analysis from an unleached whole-rock sample is nearly identical to a parallel analysis of leached material (Spitz and Boynton, 1991). For a ureilite, ALH82130 is also rich in augite and (not coincidentally) REE. However, REE-rich samples like ALH82130 would presumably dominate the REE budget

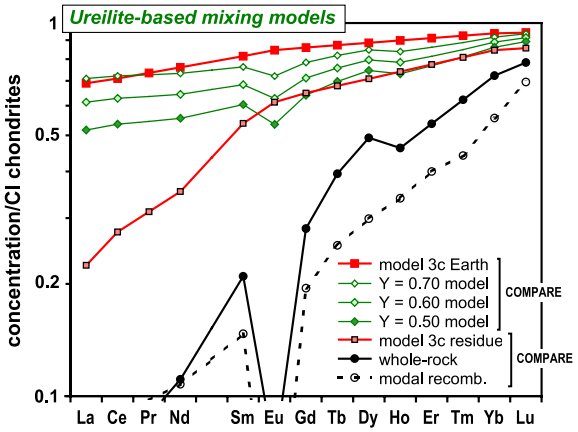


Fig. 7. The ureilite analogy: Models for REE in a planet formed as mixture of a relatively uncontaminated and appropriately high-*mg* ureilite (ALH82130, whole-rock analysis by Spitz and Boynton, 1991) with unfractionated (CI) material. These models result in Nd/Sm = 0.958, 0.971 and 0.980, for $Y = 0.50$, 0.60 and 0.70, respectively; note negative Eu anomalies. Also shown for comparison are the same "3c" model results of Figs. 3 and 4, and an average ureilite composition estimate based on modal recombination (see text) and the average mineral analyses of Guan and Crozaz (2000, 2001).

for average uncontaminated ureilite. Also, a rough modal recombination from the average mineral analyses of Guan and Crozaz (2000, 2001), assuming proportions of 68 wt% olivine, 20 wt% pigeonite, 6 wt% opx and 6 wt% augite (unfortunately, no uncontaminated data are available for the ~3 wt% of an average ureilite that is graphite-dominated "matrix"), implies a composition not very different from ALH82130 (Fig. 7). Thus, ALH82130 seems the best we can do, as a representative ureilite analog for the type of restitic planetesimal that might have engendered a depleted Earth.

Fig. 7 also shows a trio of two-component mixing models, assuming a proportion $Y$ of unfractionated CI-chondritic material mixed with $(1 - Y)$ of ALH82130 (Spitz and Boynton, 1991) composition. The results from the ureilite-based mixing models are roughly similar to the results from the model of Fig. 3c ($Y = 0.6$ variant; as merely one example out of many and diverse models that imply similar results). The final-Earth Nd/Sm implied by the ureilite-analog model is roughly 0.965–0.976 (for $Y = 0.55$–$0.65$).

One problem with the ureilite model is that a large negative Eu anomaly is implied; e.g., in the $Y = 0.6$ model, $Eu/Eu^* = 0.90$. Also, if major elements are included, Al depletions, and especially depletions in the Al/Ca ratio, are (for $Y$ values that yield major Nd/Sm fractionation) implausibly large. An average ureilite (e.g., Warren et al., 2006a) has Al ~ 0.32 × CI-chondritic, whereas Ca is 1.2 × CI. Thus, for example, in a $Y = 0.6$ model, the implied final-Earth Al is only 0.73 × CI, and the final-Earth Al/Ca is depleted to 0.67 × CI (the ureilite source materials conceivably had Al/Ca altered by aqueous fluids: Goodrich et al., 2002). The ureilites represent restites with basalt virtually removed (Guan and Crozaz, 2000; Goodrich et al., 2004; Warren et al., 2006a,b); i.e., compared to models such as that of Fig. 3c, $f$ is much higher than the $f$ at which $Eu/Eu^* \sim 1$, and the effects of this high $f$ are maximized because the residual $\Phi$ is extremely low. Even so, the ureilite analogy demonstrates that a depleted final-Earth Nd/Sm is possible, even in circumstances of abundant pigeonite, and where the $Eu/Eu^*$ turns out less than 1.

### 6.5. Wider departures from the reference model

The full range of parameter-space conceivably relevant to the hypothesis of explosive-volcanic basalt loss is too complex to cover in detail within the scope of a single paper. However, the second section of the Electronic Annex, and Tables EA-1 and EA-2, describe the effects of variation in the following parameters: $\Phi$, initial modal pyroxene/olivine ratio, initial modal pigeonite, initial modal plagioclase, the modal melting pyroxene/plag ratio, the magnitude of the unfractionated ($Y$) component, and the assumed $K_{Eu,plag}$.

### 6.6. Parameter effects generalized

One important general effect is that low-$Y$ models that result in low Nd/Sm tend to imply low final-Earth concentrations of the most highly incompatible elements, epitomized by Th (Fig. 8). The final Th concentration

Author's personal copy



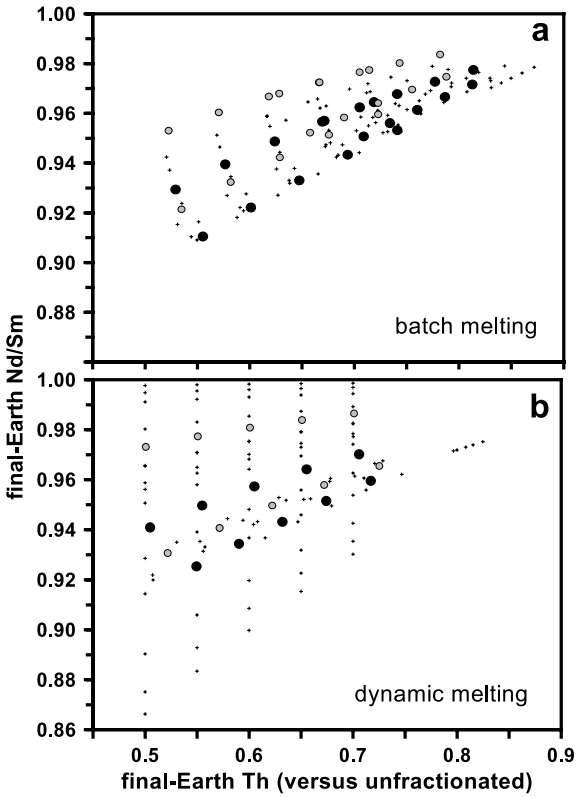


Fig. 8. Depletion of Th plotted versus final-Earth Nd/Sm for the various models tested (including $Y = 0.55$ and $Y = 0.65$ variants of the models listed in Annex Tables EA-1 and EA-2). Largest, darkest symbols denote models close to the "reference" model discussed in the text. Mid-sized symbols represent models that are analogous but assume 20 wt% initial pigeonite, or else a dubiously low porosity ($\Phi = 0.005$) for dynamic melting (b) in a planetesimal context. Smallest symbols denote models that depart most extensively from the reference model.

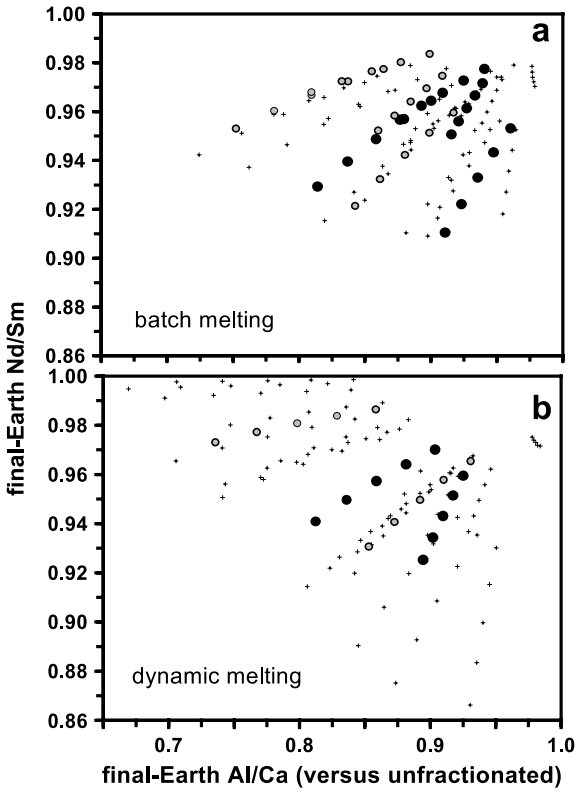


Fig. 9. Depletion of Al/Ca plotted versus final-Earth Nd/Sm for the various models tested (including $Y = 0.55$ and $Y = 0.65$ variants of the models listed in Annex Tables EA-1 and EA-2). Largest, darkest symbols denote models close to the "reference" model discussed in the text. Mid-sized symbols represent models that are analogous but assume 20 wt% initial pigeonite, or else a dubiously low porosity ($\Phi = 0.005$) for dynamic melting (b) in a planetesimal context. Smallest symbols denote models that depart most extensively from the reference model.

(normalized to unfractionated Earth-making material) is only slightly greater than $Y$; in many cases, virtually the same as $Y$. Implications for the Urey ratio and Earth's thermal evolution will be discussed below.

Among otherwise equivalent models, varying $Y$ has similar implications for Al/Ca and $Al_2O_3$ (directly proportional to Al/Ca, i.e., $\approx$1.32(Al/Ca)–0.33). However, this relationship does not translate into a general correlation between final-Earth Nd/Sm and final-Earth Al/Ca (Fig. 9). In fact, considering only dynamic-melting based models (Fig. 9b), the overall correlation between Nd/Sm and Al/Ca appears negative.

## 7. DISCUSSION

### 7.1. Likelihood of carbon-rich, anatectic earth protoplanets

The nomenclature of chondritic meteorites can be misleading. It might be inferred that ordinary noncarbonaceous chondrites are consistently carbon-poor compared to those chondrites (roughly half of all the recognized groups) that come under the heading "carbonaceous." Actually, the least thermally metamorphosed (type 3) ordinary chondrites have distinctively high C (Fig. 10). For comparison, several of the nominally carbonaceous types of chondrites, CO3, CV3 and CK (the CK value is based on only one each of types 4, 5 and 6) average 0.38, 0.54 and 0.03 wt% C, respectively (Jarosewich, 1990). Allowing for the C lost during thermal metamorphism, all of the chondrite varieties may have originally accreted into planetesimals with more than enough C (i.e., of order 0.1 wt%) to fuel major explosive-volcanic basalt loss.

The thermal evolution of the planetesimal would determine whether C was lost during gradual heating (i.e., ordinary chondrite style thermal metamorphism), or remained abundant in the mantle even during extensive anatexis, as obviously took place in the ureilite parent asteroid(s). The minimum pressure to stabilize graphite at a given $T$ and $fO_2$ can be calculated from thermodynamics, which can also be used to constrain $fO_2$ as a function of olivine composition (Fo) in the presence of metal (the thermodynamic constraints are reviewed in Warren and Kallemeyn, 1992; corroborated by some direct ureilite-simulation experiments by Walker and Grove, 1993). Combining these relationships with basic hydrostatic physics (e.g, Turcotte and Schubert, 1982), the minimum graphite-stable $P$ can be

Author's personal copy



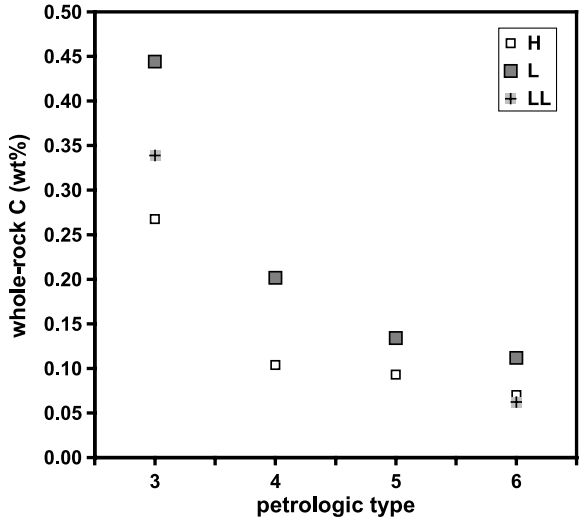


Fig. 10. Depletion of carbon by thermal metamorphism in ordinary chondrites altered from type 3 through type 6; based on averaged data from Jarosewich (1990) for 52 H, 85 L, and 19 LL chondrites.

translated into a minimum planetesimal size (radius) as a function of $T$ and olivine composition (Fig. 11). For example, the dotted curve in Fig. 11 shows one model for simultaneous growth and heating (by $^{26}$Al) of planetesimals. (The details of this heating model probably should not be taken too seriously. There are enormous uncertainties; e.g., in the original $^{26}$Al abundance. But it does serve to

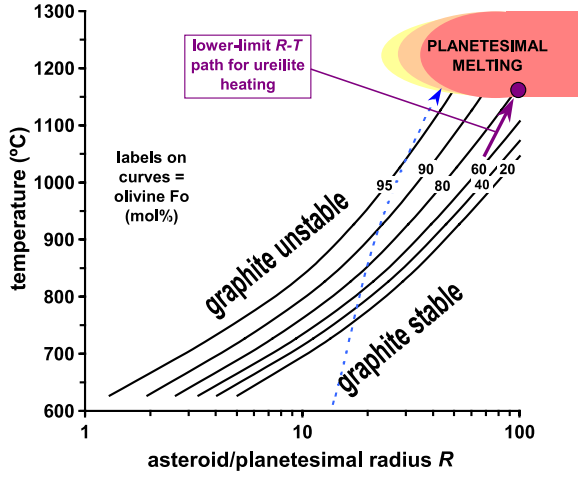


Fig. 11. The $P$–$T$–$fO_2$ stability relationships for graphite (prone to pressure- and $fO_2$-sensitive oxidation into $CO_x$ gas) in the presence of Fe-metal and mafic silicates, are here shown as a function of olivine Fo (an implicit function of $fO_2$: Warren and Kallemeyn, 1992, Fig. 6), and with $P$ translated into planetesimal radius $R$. The $P$–$R$ translation takes as reference $P$ the median $P$ (i.e., the $P$ at which half of volume is above, half below the level) within the planetesimal, assuming density is uniform at 3300 kg/m$^3$. Shown for comparison (dashed curve) is a model planetesimal heating curve from Merk et al. (2002; this is their model assuming accretion after 1.5 half lives of $^{26}$Al decay), and (heavy, solid curve) a lower limit (for $R$) heating curve implied by the genesis of ureilites as graphite-rich restites with olivines as ferroan as $Fo_{75}$.

illustrate the general expectation that planetesimals heated as they grew.) In this model, the planetesimal begins to warm within the field of graphite stability. But as it grows past ~20 km in radius, its rising $T$ being insufficiently offset by rising $P$, the planetesimal may, depending upon its redox (olivine Fo) state, begin to oxidize its graphite into fugitive $CO_x$ gas, with concomitant reduction of its mafic silicates.

Three basic scenarios are possible: (1) If thermal (and size-growth) evolution brings the planetesimal's mantle into the field of graphite instability at a $T$ below ~1200 °C, the original C content of the planetesimals would be mostly eliminated by thermal metamorphism before any melting (as apparently occurred with the ordinary chondrites: Fig. 10). The implications for C-fueled explosive-volcanic loss of basalt would be negative. (2) If the crossover into the field of graphite instability occurs at such a high $T$ that melt is present (as would be promoted by a combination of the actual heating curve being towards the right, in Fig. 11), the redox process would be a form of smelting; and if the melt component is large, the fugitive $CO_x$ gas might fuel explosive-volcanic loss of basalt as modeled above. (3) Another possibility is that most of the interior of the planetesimal, at least as long as it remains a single intact body, never enters the field of graphite instability, even though its $T$ rises into the range of silicate anatexis. The main requirement for this scenario, which is probably the most favorable for explosive-volcanic loss of basalt, would be that the heating curve extends towards the right in Fig. 11; i.e., for moderate olivine Fo, at least a few tens of kilometers to the right of the Merk et al. (2002) heating model. A clear example of this basic scenario is the case of lunar explosive volcanism (see above). However, in the planetesimal context a decisive factor may be the *mg* of the mafic silicates, as a relatively high *mg* implies a larger field of graphite stability in Fig. 11. The reduced composition (high-*mg* olivine) appropriate to Earth building material (Fo at least 88 mol% and arguably >95 mol%: Javoy, 1995, 1999) is clearly a favorable circumstance for either scenario (2) or (3), consistent with explosive-volcanic loss of basalt, and avoidance of scenario (1), pre-anatectic loss of C.

Whether the ureilites formed mainly by scenario (2) or (3) is not quite certain, but Warren et al. (2006a) cite abundant evidence in favor of (3), complicated by a late breakup of the parent asteroid(s) which abruptly diminished $P$ and thus shifted conditions into graphite instability (but also rapid cooling, which severely curtailed re-equilibration to the lower $P$). At any rate, despite having in many cases relatively ferroan mafic silicates (olivine Fo as low as 75 mol%: Mittlefehldt et al., 1998), the ureilites avoided thorough depletion of their C (an average ureilite retains a CI-like ~3 wt%: Jarosewich, 1990) while reaching $T$ high enough to completely melt (and lose) their basaltic components. In other words, the graphite "buffer" curve was crossed at $Fo_{75}$ at the highest, and the asteroid's growth and heating path must have approached the melting region with $R$ at least as high (at a given $T$) as indicated by the heavy "lower limit" arrow shown in Fig. 11.

Aside from the already discussed ordinary chondrites, other differentiated meteorites, in particular the HEDs,

Author's personal copy



demonstrate that scenario (1), and consequently volcanism with negligible graphite-fueled explosiveness, was also possible. In the thermal evolution modeling of Merk et al. (2002), a graphite-friendly low-$T/R$ trajectory on a $T$ versus $R$ plot (Fig. 11) occurs only if the planetesimal accretes with relatively low $^{26}$Al. The typical $^{26}$Al contents of the planetesimals that engendered Earth can only be guessed (cf. Hevey and Sanders, 2006; McCoy et al., 2006). Even the relevancy of $^{26}$Al to early solar system heating is still, in the view of Kunihiro et al. (2004), an open question. However, Fe- and Cr- and Al-isotopic data have recently been interpreted (Bizzarro et al., 2007) as implying that the ureilites accreted among the earliest (sampled) materials of the solar system, when $^{26}$Al was still very abundant. If so, and in view of the Merk et al. (2002) modeling, the survival of so much graphite within the post-anatexis ureilites is all the more remarkable.

### 7.2. Lunar evidence

The problem of enigmatically low planetary Nd/Sm is not altogether a new issue. As reviewed by Warren (2004), available Nd isotopic data for lunar ferroan anorthosites (the most common nonimpactite lunar highland rock type) can be interpreted as suggesting that the bulk Moon (or at least the bulk-lunar magma ocean) has Nd/Sm depleted to about $0.77 \pm 0.12$ times chondritic (see Fig. 17 of Warren, 2004). More recent results based on isotopic data for lunar basaltic rocks have led to contradictory estimates for the bulk Moon Nd/Sm, from chondritic (Rankenburg et al., 2006) to 0.81–0.86 times chondritic (Carlson and Boyet, 2006). Taylor (e.g., Taylor and Jakes, 1974; Taylor, 2001) has long advocated that the bulk Moon is enriched in refractory-lithophile elements (i.e., Al, Ca, and many incompatible elements including Th, U and the REE). However, in recent years (a) estimates for the thickness of the Moon's Al- and Ca-rich crust have been drastically lowered (Khan and Mosegaard, 2002; Lognonne, 2005), (b) the estimated global average surface Th concentration has been lowered (Warren, 2005), and most recently, (c) the heat flow estimate for one of only two locations where heat flow was measured (and preliminarily also for the other location) has been drastically lowered (Saito et al., 2007). All of these revisions point towards a bulk Moon composition that is not enriched, and might even be depleted, in refractory-lithophile elements. Conceivably, the bulk-lunar matter was considerably depleted for a few tens of millions of years before it underwent giant-impact-triggered separation from the Earth and the giant impactor body (probably mainly the latter: Canup, 2004), but was then restored to a relatively undepleted final bulk Moon composition by fractionation associated with the shallow-matter bias implied by the giant impact ejection process (i.e., the giant impact fractionation model of Warren, 1992).

### 7.3. Extremely incompatible elements and the Urey ratio

Model results (Fig. 8) indicate that a large Nd/Sm fractionation would inevitably entail a major diminution of the final-Earth concentrations of the most extremely incompatible elements, including the heat-producers Th, U and K, relative to whatever they would have been in the absence of explosive-volcanic basalt loss. This is arguably a significant drawback of the explosive-volcanic basalt loss model, because even conventional estimates for Earth's contents of these heat-producer elements have raised concerns that the Urey ratio (the ratio of the planet's internal heating rate to its surface heat flow) is improbably low (e.g., Schubert et al., 1980). This is not the place to debate the Urey ratio and planetary thermal evolution. Apart from speculations about K in the core, (past) layering of mantle convection, or the present-day global heat flow happening to be near a temporal peak, Korenaga (2006) argues that past mantle heat dissipation was probably much less efficient than customarily assumed. He points out that although mantle viscosity is largely temperature-dependent, convection tends to modulate itself by causing depletion, which in turn causes stiffening, of the upper mantle; and that this compositional stiffening may even have offset the loosening effect of the undoubtedly higher Archean $T$ (this basic notion goes back to Warren, 1984). Thus, it is unclear whether a roughly 0.7 times lower (than otherwise) Urey ratio should truly be viewed as a drawback.

A more complicated model would allow for the likelihood that the explosive-volcanic basalt loss was not neatly confined to the first stage of melting, but rather occurred sporadically throughout the eruption history of each proto-Earth-planetesimal; with a range of different detailed explosive-volcanic histories among the many planetesimals. As already discussed, to zeroeth order such a complication is probably not a major influence on the bottom-line results, as the $Y$ parameter simulates variation in the efficiency of explosive-volcanic basalt loss among a large population of protoEarth-planetesimals. However, there might be significant implications for the depletion of the extremely incompatible heat-producing elements (Fig. 8). In a dynamic melting scenario (or a scenario of multiple-batch-melting), these elements tend to leave the source and reach the planetesimal surface at a very low $X$. For example, when $f$ is 0.001 these elements are mostly already in the melt; yet 94% of the Nd, and an even higher proportion of the Sm, are still in the residual solids. Conceivably the first percent or two of melts that seep to the surface, carrying nearly all of the Th, U and K, are less efficiently dissipated by the explosive-volcanic basalt loss process compared to later melts, which arrive at a more mature variety of planetesimal surface. Efficient basalt blow-off may require that the weak, uncompacted original surface matter of the planetesimal be replaced by solid basalt—perhaps because loose material forms too wide of a volcanic orifice; or perhaps because the loose matter tends to be lofted with, and inhibit the explosive launch of, the liquid basalt droplets. Perhaps in the earliest, slowest melt percolation out of the mantle, flow was too constricted to permit efficient entrainment of graphite, the primary fuel for planetesimal explosive volcanism. Or perhaps the earliest melts that left the planetesimal mantle simply tended to be quenched by the cool near-surface material, and thus ended up largely intrusive rather than exclusively extrusive. Yet another potential

Author's personal copy



complication, tending to produce the same final result, would be if the earliest, most Th-rich, blow-off products had a greater statistical probability for reaccretion, as might be expected if the Earth-forming matter was continually accreting into a smaller and smaller number of discrete bodies, implying smaller and smaller total surface area for reaccretionary encounters. Under any of this family of (admittedly speculative) scenarios, the depletion of extremely incompatible elements, including Th, U and K, would have been dampened in relation to the quantitative modeling results presented above.

### 7.4. Other side effects of basalt loss

The Eu/Eu$^*$ ratio of an Earth formed with Nd/Sm depletion is unlikely to be perfectly chondritic. In any given partial melting model, the residual mantle's Eu/Eu$^*$ is typically well above 1 while $f$ is low, and ends well below 1 by the point of plag exhaustion, which occurs at $f = 0.167$, in reference models with 10 wt% initial plag (and plag making 60 wt% contribution to nascent melt). The behavior of Eu in the modeling is sensitive to the assumed $K_{Eu,plag}$, which (as discussed in Section 5) is uncertain, and possibly closer to 1.1 than to the "reference" value of 0.7. Based on numerical integration of all the reference models ($K_{Eu,plag} = 0.7$, $Y = 0.5$–$0.7$, etc.) through the melting range 3 wt% $< X <$ 14 wt%, the average final-Earth Eu/Eu$^*$ is $\sim 0.995 \pm$ (one-$\sigma$) 0.029. However, if instead $K_{Eu,plag}$ is assumed to be 1.1, this result shifts to $1.035 \pm 0.038$. Thus, a $K_{Eu,plag} = 1.1$ variant of the overall model would imply a significant likelihood for Eu/Eu$^*$ to be mildly superchondritic (e.g., a 25% chance for Eu/Eu$^*$ to be greater than 1.06 times chondritic).

The implied roughly 10–15% reduction in Earth's Al/Ca (Fig. 9) is arguably an important advantage. As first noted by Palme and Nickel (1985), in most mantle periodtites the Al/Ca ratio is distinctly subchondritic; the average in a recent data compilation (Lyubetskaya and Korenaga, 2007) is $\sim$0.85 times chondritic. Explosive-volcanic basalt loss might also cause a slight diminution in Si/Mg. However, this effect is difficult to quantify. The $SiO_2$ content of the basalt lost in the models is 58–60 wt%, depending upon the (melting) plag/pyroxene ratio and the detailed compositions of the (melting) plag and pyroxene. But potential starting compositions, judging from the nonmetallic, nonsulfide fractions of chondritic meteorites, have $SiO_2$ ranging from 36 (CI) to 59 (EH) wt% (Jarosewich, 1990).

The explosive-volcanic basalt loss model implies a considerable diminution in Hf/Lu, to 0.75–0.92 (relative to unfractionated–chondritic) in typical, near-reference models (Annex Fig. EA-2). This result is broadly consistent with Boyet and Carlson (2006) inference that Hf/Lu (weight ratio) in the "early depleted reservoir" (EDR) portion of the mantle is $\sim$3.7. However, Caro et al. (2005) and Bennett et al. (2007) have adduced evidence that the bulk-Earth Hf/Lu precisely matches the chondritic average (4.2; i.e., $^{176}Lu/^{177}Hf = 0.0332$). Unfortunately, quantitative comparison, model versus Earth, is difficult, because unlike Nd/Sm or Al/Ca, Hf/Lu is far from constant among chondrites. Patchett et al. (2004), noting that Hf/Lu ranges among chondrites by 30% including all high-precision (isotope-dilution) literature data, concluded "it is not possible to select...BSE [bulk-silicate Earth] parameters for Lu–Hf except on a subjective basis."

The focus in this paper has been on basalt loss by the explosive-volcanic mechanism. However, as noted by Goldstein et al. (2006), similar basalt (crust) depletion effects conceivably resulted from incomplete disruption of differentiated planetesimals during "hit-and-run collisions" of the type postulated by Asphaug et al. (2006). Collisional silicate (as opposed to metal-silicate) differentiation warrants further study. In order to engender a significant net depletion (in the Nd/Sm sense) in a terrestrial planet, collisions would have to systematically, among a large number of planetesimals, favor more thorough dispersal (into small bodies that avoid reaccretion into the bodies that eventually form the planet) of the near-surface crustal layers in comparison to the mantles. If such was the case, the net geochemical effects would have been analogous to, and possibly reinforcing of, those modeled above.

## 8. SUMMARY AND CONCLUSIONS

The common assumption that the bulk-Earth composition must be chondritic for refractory-lithophile elements, a category that includes the REE, Th, U, and the major elements $Al_2O_3$ and CaO, is dubious. Assuming that the mantles of Earth-building planetesimals of order 100 km in diameter tended to undergo anatexis while retaining abundant carbon, as occurred within at least one meteorite parent asteroid, pressure-sensitive oxidation of the carbon in ascending magmas would have fueled explosive launch of basalt melt droplets, often to such high velocity that they became gravitationally unattached to the planetesimal. The inevitable result, given this scenario, would be depletion of ratios such as Nd/Sm in the residual planetesimal.

Assuming the melt droplets were comparable in size to lunar pyroclastic droplets, there would be little chance for reaccretion to the parent planetesimal, because size-sensitive drag effects (e.g., Poynting–Robertson) would quickly modify the droplet orbits. Less clear (needing further study) is whether these particles would mostly spiral into the Sun, or reaccrete onto other protoEarth-planetesimals.

Given the premise of anatexis within small, carbon-rich planetesimals, major uncertainties that affect the degree of final-Earth depletion include the extent of basalt loss, the mineralogy of the initial source matter, and the physical style of melting during the genesis of the basalt. The overall extent of basalt loss has been modeled by assuming various combinations of $X$ (the extent of basalt removed from a given planetesimal) and $Y$, the proportion of the planet assumed (for modeling purposes) to consist of entirely unfractionated material.

The most plausible initial mineral assemblage for proto-Earth planetesimals, given the reduced nature of this planet (high proportion of Fe-metal, coupled with high oxide *mg* ratio), has 30–50 wt% olivine, 39–59 wt% pyroxene, 10 wt% plagioclase and 1 wt% opaque oxides; the pyroxene is an 80:20 mix of orthopyroxene and high-Ca pyroxene. Models based on this reference mineralogy result in a substantially fractionated final-Earth Nd/Sm, typically in the

Author's personal copy



range 0.93–0.96 times the unfractionated (chondritic) ratio, assuming moderate $X$ (or $f$) and $Y$.

In general, a high pyroxene/olivine ratio results in a higher degree of final-Earth Nd/Sm fractionation. Substituting pigeonite for some of the opx + high-Ca pyroxene of the reference model tends to result in dampened final-Earth Nd/Sm fractionation.

For any given initial mineralogy, models predicated on batch-style partial melting are most effective, in terms of yielding fractionated final-Earth Nd/Sm, if the residual porosity after melt segregation is assumed to be small. The opposite holds for models predicated on dynamic-style partial melting: a high residual porosity during melting translates (over most of the plausible range in $X$) into a higher degree of final-Earth Nd/Sm fractionation.

Important final-Earth side effects of basalt loss by explosive volcanism include highly depleted contents of the heat-generating elements, Th, U and K (caveat: this effect might be dampened if, for various potential reasons, the earliest ~1% of basalt generated tended to be dissipated less efficiently); a depleted Al/Ca ratio; a depleted Hf/Lu ratio; and a small but conceivably noticeable Eu anomaly. Better constraints on the relevant $K_{Eu,plag}$ (i.e., at low $fO_2$ but also moderate plag Na/Ca ratio), along with a fresh, meticulous assessment of the bulk-Earth $Eu/Eu^*$, could conceivably lead to significant insight regarding the extent of basalt loss during the growth of Earth from planetesimals.

It is certainly debatable whether basalt loss by explosive volcanism resulted in sufficient Nd/Sm fractionation, to ~0.932 times chondritic, to engender the full 20 μ of $^{142}Nd/^{144}Nd$ excess inferred for the "early depleted reservoir" by Boyet and Carlson (2006). However, modeling suggests that basalt loss by explosive volcanism not only takes Nd/Sm in that direction, but also tends to yield roughly that degree of fractionation. Given the high-precision of modern isotopic measurements and isotopic-tracer modeling, it does not appear likely that Earth's building block planetesimals evolved with basalt loss by explosive volcanism so consistently inefficient that the effects on final-Earth ratios such as Nd/Sm were negligible.

## ACKNOWLEDGMENTS

I am indebted to G.J. Taylor and Anonymous for helpful reviews, and the Associate Editor (D.W.M.) for additional helpful suggestions. I also thank M.A. Jura for advice on interplanetary-dust drag effects, and D.T. Vaniman for sharing SEM images of lunar tuff rocklet 72504,10. Although I had been intending to assay the broader planetary implications of basalt loss by explosive volcanism for many years, actual work on a paper was stimulated by (apart from Boyet and Carlson, 2006; Saito et al., 2007) discussions with T.M. Harrison, K.D. McKeegan, D.J. Taylor and H. Zou. This research was supported by NASA Grant NAG5-4215.

## APPENDIX A. SUPPLEMENTARY DATA

Supplementary data associated with this article can be found, in the online version, at doi:10.1016/j.gca.2007.11.038.

## REFERENCES

Albarède F. (2006) Isotopic hide and seek. *Nature* **444**, 162.

Arai T. and Warren P. H. (1999) Lunar meteorite QUE94281: glass compositions and other evidence for launch pairing with Yamato-793274. *Meteorit. Planet. Sci.* **34**, 209–234.

Arndt J. and von Englehardt W. (1987) Formation of Apollo 17 orange and black glass beads. *Proc. Lunar Planet. Sci. Conf.* **17**, E372–E376.

Asphaug E., Agnor C. B. and Williams Q. (2006) Hit-and-run planetary collisions. *Nature* **439**, 155–160.

Beard B. L., Taylor L. A., Scherer E. E., Johnson C. M. and Snyder G. A. (1998) The source region and melting mineralogy of high-titanium amd low-titanium lunar basalts deduced from Lu–Hf isotope data. *Geochim. Cosmochim. Acta* **62**, 525–544.

Bennett V. C., Brandon A. D., Hiess J. and Nutman A. P. (2007) Coupled $^{142}Nd$, $^{143}Nd$ and $^{176}Hf$ isotopic data from 3.6–3.9 Ga rocks: new constraints on the timing and composition of early terrestrial chemical reservoirs. *Lunar Planet. Sci.* **38** Abstract #2139.

Bizzarro M., Baker J. A., Haack H. and Lundgaard K. L. (2005) Rapid timescales for accretion and melting of differentiated planetesimals inferred from $^{26}Al$–$^{26}Mg$ chronometry. *Astrophys. J.* **63**, L41–L44.

Bizzarro M., Ulfbeck D., Trinquier A., Thrane K., Connelly J. N. and Meyer B. S. (2007) Evidence for a late supernova injection of $^{60}Fe$ into the protoplanetary disk. *Science* **316**, 1178–1181.

Bourdon B., Ribe N. M., Stracke A., Saal A. E. and Turner S. P. (2006) Insights into the dynamics of mantle plumes from uranium-series geochemistry. *Nature* **444**, 713–717.

Boyet M. and Carlson R. W. (2005) $^{142}Nd$ evidence for early (>453 Ga) global differentiation of the silicate Earth. *Science* **309**, 576–581.

Boyet M. and Carlson R. W. (2006) A new geochemical model for the Earth's mantle inferred from $^{146}Sm$–$^{142}Nd$ systematics. *Earth Planet. Sci. Lett.* **250**, 254–268.

Boyet M., Blichert-Toft J., Rosing M., Storey M., Telouk P. and Albarede F. (2003) $^{142}Nd$ evidence for early Earth differentiation. *Earth Planet. Sci. Lett.* **214**, 427–442.

Brophy J. G. and Basu A. (1990) Europium anomalies in mare basalts as a consequence of mafic cumulate fractionation from an initial lunar magma. *Proc. Lunar Planet. Sci. Conf.* **20**, 25–30.

Cameron A. G. W. (1995) The first ten million years in the solar nebula. *Meteoritics* **30**, 133–161.

Canup R. M. (2004) Dynamics of lunar formation. *Annu. Rev. Astron. Astrophys.* **42**, 441–475.

Carlson R. W. and Boyet M. (2006) Evidence for a strongly depleted early Earth. *American Geophys. Union Fall Meeting 2006*, Abstract #V22C-07.

Caro G., Bourdon B., Birck J. L. and Moorbath S. (2003) $^{146}Sm$–$^{142}Nd$ evidence from Isua metamorphosed sediments for early differentiation of the Earth's mantle. *Nature* **423**, 428–432.

Caro G., Bourdon B., Wood B. J. and Corgne A. (2005) Trace-element fractionation in Hadean mantle generated by melt segregation from a magma ocean. *Nature* **436**, 246–249.

Cataldo E., Wilson L., Lane S. and Gilbert J. (2002) A model for large-scale volcanic plumes on Io: implications for eruption rates and interactions between magmas and near-surface volatiles. *J. Geophys. Res.* **107**(E11), 19-1–19-12.

Chase C. G. and Patchett P. J. (1988) Stored mafic/ultramafic crust and early Archean mantle depletion. *Earth Planet. Sci. Lett.* **91**, 66–72.

Delano J. W. (1986) Pristine lunar glasses: criteria, data, and implications. *Proc. Lunar Planet. Sci. Conf.* **16**, D201–D213.

Author's personal copy



Dube A., Fredriksson B. J., Jarosewich E., Nelen J. A., Noonan A. F., O'Keefe J. and Fredriksson K. (1977) Eight L-group chondrites: a comparative study. *Smithson. Contrib. Earth Sci.* **19**, 71–82.

Floss C. (2000) Complexities on the acapulcoite–lodranite parent body: evidence from trace element distributions in silicate minerals. *Meteorit. Planet. Sci.* **35**, 1073–1085.

Fogel R. A. (2005) Aubrite basalt vitrophyres: the missing basaltic component and high-sulfur silicate melts. *Geochim. Cosmochim. Acta* **69**, 1633–1648.

Fredriksson K., Dube A., Jarosewich E., Nelen J. and Noonan A. (1975) The Pulsora anomaly: a case against metamorphic equilibration in chondrites. *Smithson. Contrib. Earth Sci.* **14**, 41–53.

Goldstein J. I., Yang J., Scott E. R. D., Taylor G. J. and Asphaug E. (2006) Implications of hit-and-run collisions between differentiated protoplanets: evidence from iron meteorites. In *Workshop on Early Planetary Differentiation: A Multi-Planetary and Multi-Disciplinary Perspective* (eds. C. Shearer, L. Borg and K. Righter), Abstract #4037. Lunar and Planetary Institute.

Goodrich C. A., Krot A. N., Scott E. R. D., Taylor G. J., Fioretti A. M. and Keil, K. (2002) Formation and evolution of the ureilite parent body and its offspring. *Lunar Planet. Sci.* **33**, Abstract #1379.

Goodrich C. A., Scott E. R. D. and Fioretti A. M. (2004) Ureilitic breccias: clues to the petrologic structure and impact disruption of the ureilite parent asteroid. *Chem. Erde* **64**, 283–327.

Guan Y. and Crozaz G. (2000) Light rare earth enrichments in ureilites: a detailed ion microprobe study. *Meteorit. Planet. Sci.* **35**, 131–144.

Guan Y. and Crozaz G. (2001) Microdistributions and petrogenetic implications of rare earth elements in polymict ureilites. *Meteorit. Planet. Sci.* **36**, 1039–1056.

Hevey P. and Sanders I. S. (2006) A model for planetesimal meltdown by $^{26}$Al and its implications for meteorite parent bodies. *Meteorit. Planet. Sci.* **41**, 95–106.

Holzheid A. and Grove T. L. (2002) Sulfur saturation limits in silicate melts and their implications for core formation scenarios for terrestrial planets. *Am. Mineral.* **87**, 227–237.

Hutchison R., Bevan A. W. R., Easton A. J. and Agrell S. O. (1981) Mineral chemistry and genetic relations among H-group chondrites. *Proc. R. Soc. Lond. A Math. Phys. Sci.* **374**, 159–178.

Jarosewich E. (1990) Chemical analyses of meteorites: a compilation of stony and iron meteorite analyses. *Meteoritics* **25**, 323–337.

Javoy M. (1995) The integral enstatite chondrite model of the Earth. *Geophys. Res. Lett.* **22**, 2219–2222.

Javoy M. (1999) Chemical Earth models. *C. R. Acad. Sci. (Paris)* **329**, 537–555.

Keil K. (1989) Enstatite meteorites and their parent bodies. *Meteoritics* **24**, 195–208.

Kennedy A. K., Lofgren G. E. and Wasserburg G. J. (1993) An experimental study of trace element partitioning between olivine, orthopyroxene, and melt in chondrules. *Earth Planet. Sci. Lett.* **115**, 177–195.

Khan A. and Mosegaard K. (2002) An inquiry into the lunar interior: a nonlinear inversion of the Apollo lunar seismic data. *J. Geophys. Res. Planets* **107**(E6), 3.1–3.23.

Kita N. T., Ikeda Y., Togashi S., Liu Y., Morishita Y. and Weisberg M. K. (2004) Origin of ureilites inferred from a SIMS oxygen isotopic and trace element study of clasts in the Dar al Gani 319 polymict ureilite. *Geochim. Cosmochim. Acta* **68**, 4213–4235.

Korenaga J. (2006) Archean geodynamics and the thermal evolution of Earth. In *Archean Geodynamics and Environments* (eds. J. Korenaga, K. Benn, J.-C. Mareschal and K. C. Condie), pp. 7–32. American Geophysical Union, Geophysical Monograph 164.

Krauss O., Wurm G., Mousis O., Petit J.-M., Horner J. and Alibert Y. (2007) The photopheretic sweeping out of dust in transient protoplanetary disks. *Astron. Astrophys.* **462**, 977–987.

Kunihiro T., Rubin A. E., McKeegan K. D. and Wasson J. T. (2004) Initial $^{26}$Al/$^{27}$Al in carbonaceous-chondrite chondrules: too little $^{26}$Al to melt asteroids. *Geochim. Cosmochim. Acta* **68**, 2947–2957.

Lee C.-T. A., Harbert A. and Leeman W. P. (2007) Extension of lattice strain theory to mineral/mineral rare-earth element partitioning: internally consistent partition coefficients between olivine, orthopyroxene, clinopyroxene and basaltic melt. *Geochim. Cosmochim. Acta* **71**, 481–496.

Libourel G., Marty B. and Humbert F. (2003) Nitrogen solubility in basaltic melt Part I. Effect of oxygen fugacity. *Geochim. Cosmochim. Acta* **67**, 4123–4135.

Lognonne P. (2005) Planetary seismology. *Ann. Rev. Earth Planet. Sci.* **33**, 571–604.

Longhi J. and Pan V. (1988) A reconnaissance study of phase boundaries in low-alkali basaltic liquids. *J. Petrol.* **29**, 115–147.

Lyubetskaya T. and Korenaga J. (2007) Chemical composition of Earth's primitive mantle and its variance, 1: method and results. *J. Geophys. Res.* **112**, B03211, doi:10.1029/2005JB004223.

Maaløe S. (1982) Geochemical aspects of permeability-controlled partial melting and fractional crystallization. *Geochim. Cosmochim. Acta* **46**, 43–57.

McCoy T. J., Mittlefehldt D. W. and Wilson L. (2006) Asteroid differentiation. In *Meteorites and the Early Solar System II* (eds. DS. Lauretta and HY. McSween). University of Arizona Press, pp. 733–745.

McKay G. A. (1989) Partitioning of rare earth elements between major silicate minerals and basaltic melts. *Rev. Mineral. Geochem.* **21**, 45–77.

McKay G. A., Wagstaff J. and Yang S.-R. (1986) Clinopyroxene REE distribution coefficients for shergottites: the REE content of the Shergotty melt. *Geochim. Cosmochim. Acta* **50**, 927–937.

McKay G., Le L. and Wagstaff J. (1991) Constraints on the origin of the mare basalt europium anomaly: REE partition coefficients for pigeonite. *Lunar Planet. Sci.* **22**, 883–884.

Merk R., Breuer D. and Spohn T. (2002) Numerical modeling of $^{26}$Al-induced radioactive melting of asteroids considering accretion. *Icarus* **159**, 183–191.

Mittlefehldt D. W., McCoy T. J., Goodrich C. A. and Kracher A. (1998) Non-chondritic meteorites from asteroidal bodies. *Rev. Mineral. Geochem.* **36**, 4.1–4.195.

Mueller R. F. and Olsen E. J. (1967) The olivine, pyroxene, and metal content of chondritic meteorites as a consequence of Prior's rule. *Mineral. Mag.* **36**, 311–318.

Mukai T. and Yamamoto T. (1982) Solar wind pressure on interplanetary dust. *Astron. Astrophys.* **107**, 97–100.

Nakamura Y., Fujimaki H., Nakamura N. and Tatsumoto M. (1986) Hf, Zr, and REE partition coefficients between ilmenite and liquid: implications for lunar petrogenesis. *Proc. Lunar Planet. Sci. Conf.* **16**, D239–D250.

Norman M. D., Garcia M. O. and Pietruszka A. J. (2005) Trace-element distribution coefficients for pyroxenes, plagioclase, and olivine in evolved tholeiites from the 1955 eruption of Kilauea Volcano. *Am. Mineral.* **90**, 888–899.

Palme H. and Nickel K. G. (1985) Ca/Al ratio and composition of the Earth's upper mantle. *Geochim. Cosmochim. Acta* **49**, 2123–2132.

Patchett P. J., Vervoort J. D., Söderlund U. and Salters V. J. M. (2004) Lu–Hf and Sm–Nd isotopic systematics in chondrites

Author's personal copy



and their constraints on the Lu–Hf properties of the Earth. *Earth Planet. Sci. Lett.* **222**, 29–41.

Rankenburg K., Brandon A. D. and Neal C. R. (2006) Neodymium isotope evidence for a chondritic composition of the Moon. *Science* **312**, 1369–1372.

Robertson H. P. (1937) Dynamical effects of radiation in the solar system. *Mon. Not. R. Astron. Soc.* **97**, 423–438.

Ryabova G. O. (2005) On the dynamical consequences of the Poynting–Robertson drag caused by solar wind. In *Dynamics of Populations of Planetary Systems, IAU Colloquium No. 197* (eds. Z. Knezevic and A. Milani), pp. 411–414. International Astronomical Union.

Saito Y., Tanaka S., Takita J., Horai K. and Hagermann, A. (2007) Lost Apollo heat flow data suggest a different lunar bulk composition. *Lunar Planet. Sci.* **38**, Abstract #2197.

Samuel H. and Farnetani C. G. (2003) Thermochemical convection and helium concentrations in mantle plumes. *Earth Planet. Sci. Lett.* **207**, 39–56.

Sato M. (1979) The driving mechanism of lunar pyroclastic eruptions inferred from the oxygen fugacity behavior of Apollo 17 orange glass. *Proc. Lunar Planet. Sci. Conf.* **10**, 311–325.

Schubert G., Stevenson D. and Cassen P. (1980) Whole planet cooling and the radiometric heat source contents of the earth and the moon. *J. Geophys. Res.* **85**, 2531–2538.

Scott E. R. D., Taylor J. G. and Keil K. (1993) Origin of ureilite meteorites and implications for planetary accretion. *Geophys. Res. Lett.* **20**, 415–418.

Shaw D. M. (2000) Continuous (dynamic) melting theory revised. *Can. Mineral.* **38**, 1041–1063.

Shearer C. K. and Papike J. J. (1993) Basaltic magmatism on the Moon: a perspective from volcanic picritic glass beads. *Geochim. Cosmochim. Acta* **57**, 4785–4812.

Sims K. W. W., DePaolo D. J., Murrell M. T., Baldridge W. S., Goldstein S., Clague D. and Jull M. (1999) Porosity of the melting zone and variations in the solid mantle upwelling rate beneath Hawaii: inferences from $^{238}$U–$^{230}$Th–$^{226}$Ra and $^{235}$U–$^{231}$Pa disequilibria. *Geochim. Cosmochim. Acta* **63**, 4119–4138.

Spitz A. H. and Boynton W. V. (1991) Trace element analysis of ureilites: new constraints on their petrogenesis. *Geochim. Cosmochim. Acta* **55**, 3417–3430.

Sun C.-O., Williams R. J. and Sun S.-S. (1974) Distribution coefficients of Eu, Sr for plagioclase-liquid and clinopyroxene-liquid equilibria in an oceanic ridge basalt: an experimental study. *Geochim. Cosmochim. Acta* **38**, 1415–1433.

Taylor G. J., Keil K., McCoy T., Haack H. and Scott E. R. D. (1993) Asteroid differentiation: pyroclastic volcanism to magma oceans. *Meteorit. Planet. Sci.* **28**, 34–52.

Taylor S. R. (2001) *Solar System Evolution*, second ed. Cambridge University Press.

Taylor S. R. and Jakes P. (1974) The geochemical evolution of the Moon. *Proc. Lunar Sci. Conf.* **5**, 1287–1305.

Tolstikhin I. N., Kramers J. D. and Hofmann A. W. (2006) A chemical Earth model with whole mantle convection: the importance of a core-mantle boundary layer (D″) and its early formation. *Chem. Geol.* **226**, 79–99.

Turcotte D. L. and Schubert G. (1982) *Geodynamics: Applications of Continuum Physics to Geological Problems*. Wiley.

Urey H. C. (1952) The origin and development of the earth and other terrestrial planets: a correction. *Geochim. Cosmochim. Acta* **2**, 263–268.

Walker D. and Grove T. (1993) Ureilite smelting. *Meteoritics* **28**, 629–636.

Warren P. H. (1984) Primordial degassing, lithosphere thickness, and the origin of komatiites. *Geology* **12**, 335–338.

Warren P. H. (1992) Inheritance of silicate differentiation during lunar origin by giant impact. *Earth Planet. Sci. Lett.* **112**, 101–116.

Warren P. H. (2004) The Moon. In *Treatise on Geochemistry*, vol. 1 (ed. A. M. Davis), pp. 559–599. Meteorites, Comets and Planets. Elsevier.

Warren P. H. (2005) New lunar meteorites: implications for composition of the global lunar surface, of the lunar crust, and of the bulk Moon. *Meteorit. Planet. Sci.* **40**, 477–506.

Warren P. H. and Kallemeyn G. W. (1992) Explosive volcanism and the graphite-oxygen fugacity buffer on the parent asteroid(s) of the ureilite meteorites. *Icarus* **100**, 110–126.

Warren P. H., Huber H. and Ulff-Møller F. (2006a) Alkali-feldspathic material entrained in Fe,S-rich veins in a monomict ureilite. *Meteorit. Planet. Sci.* **41**, 797–813.

Warren P. H., Ulff-Møller F., Huber H. and Kallemeyn G. W. (2006b) Siderophile geochemistry of ureilites: a record of early stages of planetesimal core formation. *Geochim. Cosmochim. Acta* **70**, 2104–2126.

Wasson J. T. (1977) Relationship between the composition of solid solar-system matter and distance from the Sun. In *Comets, Asteroids and Meteorites: Interrelations, Evolution and Origins* (ed. A. H. Delsemme), pp. 551–559. University of Toledo.

Wasson J. T. and Kallemeyn G. W. (1988) Compositions of chondrites. *Philos. Trans. R. Soc. Lond.* **A325**, 535–544.

Weitz C. M., Rutherford M. J., Head, III, J. W. and McKay D. S. (1999) Ascent and eruption of a lunar high-titanium magma as inferred from the petrology of the 74001/2 drill core. *Meteorit. Planet. Sci.* **34**, 527–540.

Wetherill G. W. (1967) Collisions in the asteroid belt. *J. Geophys. Res.* **72**, 2429–2444.

Wilson L. and Keil K. (1991) Consequences of explosive eruptions on small Solar System bodies: the case of the missing basalts on the aubrite parent body. *Earth Planet. Sci. Lett.* **104**, 505–512.

Wilson L. and Keil K. (1997) The fate of pyroclasts produced in explosive eruptions on the asteroid 4 Vesta. *Meteorit. Planet. Sci.* **32**, 813–823.

Wood J. A. (2000) Pressure and temperature profiles in the solar nebula. *Space Sci. Rev.* **92**, 87–93.

Wyatt, Jr., S. P. and Whipple F. L. (1950) The Poynting–Robertson effect on meteor orbits. *Astrophys. J.* **111**, 134–141.

Zahnle K. J. (2006) Earth's earliest atmosphere. *Elements* **2**, 217–222.

Zolotov M. Y. and Fegley B. (1999) Oxidation state of volcanic gases on Io. *Lunar Planet. Sci.* **30**, Abstract #1132.

Zou H. (2007) *Quantitative Geochemistry*. Imperial College Press.

Zou H. B. (2000) Trace element fractionation during modal and nonmodal dynamic melting and open-system melting: a mathematical treatment. *Geochim. Cosmochim. Acta* **62**, 1937–1945.

*Associate editor:* David W. Mittlefehldt